How much of a machine-learning earthquake catalogue can an expert verify?

Lingsen Meng[1,*], Hui Huang[2,†], Jinzhi Ma[3,†], Yang Ma[1,†]

[1]Department of Earth, Planetary, and Space Sciences, University of California, Los Angeles, CA, USA
[2]School of Ocean and Earth Science, Tongji University, Shanghai, China
[3]Institute of Geology and Geophysics, Chinese Academy of Sciences, Beijing, China

[*]Corresponding author: lsmeng@g.ucla.edu
[†]These authors contributed equally.

This is a non-peer-reviewed preprint submitted to EarthArXiv. The manuscript has been submitted to a journal for peer review; any subsequent versions may differ.

Abstract.
Machine-learning systems are becoming the instruments that generate the primary data of a scientific field, and what such a system asserts is not the same as what an expert would endorse. Earthquake detection is one of the few settings where the difference can be measured, because a detection can be checked blind against the waveforms that produced it. Four seismologists returned 4,800 blind verdicts on 1,200 detections from six catalogues. Of the events they were willing to judge they confirmed 60 to 98%, and three catalogues of the same Ridgecrest sequence, judged from the same waveforms, differed by ~20 points. A score fitted to seven quantities a catalogue already records reproduces the panel, transfers to a sequence it was not trained on, and ranks the machine-only additions lowest. Measuring this link, and re-measuring it as the systems change, keeps human judgement inside the scientific record rather than upstream of it.
One-sentence summary. Four seismologists judging waveforms blind endorse 60 to 98% of a machine-learning earthquake catalogue, and a score fitted to what the catalogue already records reproduces their judgement.

Introduction

Machine-learning systems are increasingly the instruments that produce the primary observational data of a scientific field, rather than tools applied to data that were collected some other way. However, the rate at which a domain expert would endorse what such a system asserts is, in most fields, not measured, largely because the raw evidence behind an individual machine output is either unavailable or too costly for a person to review. Seismology is an exception on both counts, and that is why we take it as the setting for this measurement. An earthquake detection is a claim about a specific set of waveforms, those waveforms are archived and public, and a trained seismologist can look at them and decide whether the claim is supported. In addition, that check can be blinded, since the record section can be shown with the origin time, location, depth and magnitude removed, so the verdict cannot be contaminated by the catalogue's own claims. Thus the question of how much of a machine-generated data set an expert will endorse, which is elsewhere a matter of opinion, becomes here a quantity that can be measured, and re-measured as the systems change.

Deep-learning phase pickers have changed the scale of observational seismology[1]. Networks such as PhaseNet[2], EQTransformer[3] and their successors detect arrivals far below the amplitude at which a human analyst can identify them visually, and the catalogues built from them contain five to fifty times more events than the routine catalogues they extend[4-9]. These catalogues are no longer a methodological curiosity. They are the input to studies of fault-zone architecture, foreshock sequences and aftershock decay, they are being taken up in earthquake forecasting[10,11] as fast as they are produced, and they are increasingly distributed as community data products in their own right.

The step that has not kept pace is verification. A detection enters a machine-learning catalogue when an associator finds a set of picks consistent with a hypocentre, and nothing in that chain establishes that an earthquake produced them. Feeding the same associator picks whose times have been shuffled within the day returns more events than the real data does (Note S2), so the fact that an associator produced an event is not by itself evidence that anything seismic occurred. Two failure modes pass its consistency check without a source: one earthquake can be associated twice at slightly different origin times, and unrelated noise picks can happen to fit a common hypocentre. The usual checks, i.e. agreement with an independent catalogue, a signal-to-noise threshold or a magnitude-of-completeness argument, measure something adjacent to the question. Two studies have come closest. Noel and West[12] compared machine-learning, real-time and analyst-reviewed catalogues of several Alaskan regions and found that the machine catalogue introduced misidentified non-earthquake signals, and Herrmann and Marzocchi[13] showed that high-resolution catalogues depart systematically from the Gutenberg–Richter law at low magnitude and traced the departures to mixed magnitude types, inhomogeneous completeness and processing artefacts. Neither was a systematic, blind review of the detections themselves, so neither gives a rate of false detections that transfers to another catalogue.

The consequence of lacking systematic event review is that a quantity everyone depends on is unmeasured. When a study reports a b-value from 10^5 machine-detected events, or infers fault geometry from their spatial distribution, the analysis proceeds as though the catalogue were a list of earthquakes. If a substantial fraction are not, the inference inherits an error that no amount of care downstream can remove, because the error is in the data and not in the analysis.

Here we use that opportunity and ask four questions. How much of a machine-learning catalogue can an expert verify? Is that fraction a property of the earthquake sequence or of the pipeline that catalogued it? Can the expert judgement be reproduced automatically, and if so, what does a machine have to be given to reproduce it? And, the question that decides whether any of this matters, do the detections an expert cannot verify carry a systematically higher chance of being false?

Results

What a reviewer sees

We audited eight automated catalogues of six earthquake sequences (Table S1). The six sequences span tectonic, subduction, volcanic and induced seismicity, and more than two orders of magnitude in scale, from a 3 km hydraulic-fracture network at ToC2ME, whose catalogue is built by beamforming rather than by a neural picker, to an 800 km slab beneath NE Japan. Three of the six we built ourselves from continuous waveforms, picking with PhaseNet, associating with PyOcto and locating with ADLoc: Ridgecrest, Iquique and Kīlauea. The other three, Amatrice, the NE Japan forearc and ToC2ME, are published community catalogues audited exactly as their authors distribute them, so the audit measures the products the community actually uses. One catalogue of each sequence was judged by the full panel of four reviewers. Two additional catalogues of the Ridgecrest sequence, built by other groups from the same waveforms, were judged by one of the four reviewers (Methods).

A random draw of 200 events from a catalogue of 10^5 would be dominated by its most common kind of event and would say almost nothing about the rare kinds, so from each catalogue we drew a stratified sample of 200 events on variables the catalogue itself records, e.g. the number of associated phases and the magnitude, and weighted every verdict back by the number of catalogue events its stratum holds (Methods). Each event was rendered as a record section with everything the catalogue asserts about it removed from the image, i.e. the origin time, the location, the depth, the magnitude and the station names (Fig. 1). A reviewer sees the five nearest stations in order of distance, labelled only by that rank, with a predicted P and S from a straight-ray model, and nothing else. The three examples in Fig. 1 span the scale the panel used: an impulsive onset at the predicted P on every row with a consistent S move-out (confirmed); an onset present on the distant rows but overprinted on the nearest ones by a larger event a few seconds later, which is the situation in which reviewers most often declined to decide (unresolved); and a catalogue entry carrying a magnitude of 2.6 with nothing coherent at the prediction on any station, assembled by the associator from picks in a busy coda (rejected). Four seismologists returned a verdict on this three-way scale for every event of the six sequence panels, which gives 4,800 verdicts in a fully crossed design.

How much of each catalogue an expert will stand behind

The four verdicts on each event are combined into a single label by plurality, with a two-against-two split counted as unresolved (Methods), and the labels are weighted back to the catalogue (Fig. 2a). Among the detections the panel was willing to decide, the confirmed fraction is 97.6% at Kīlauea, 97.3% at Iquique, 95.5% at Amatrice, 85.3% at Ridgecrest, 84.1% in the NE Japan forearc and 60.1% at ToC2ME (Fig. 2b and Table S9). The median is 90.4%, and the spread is nearly forty percentage points across six catalogues that were all built to the standards of the field.

The confirmed fraction is not a single number, because reviewers decline a substantial share of events, and the honest statement is a range. At Ridgecrest 31.1% of the catalogue weight sits on events the panel would not call either way, so counting those as rejected or as confirmed puts the confirmed share at 58.7% or 89.8%. The corresponding range at ToC2ME runs from 42.4% to 71.8% (Fig. 2b). A second convention matters almost as much: 22 of the 200 Ridgecrest events split two against two, and counting those ties as rejected rather than confirmed moves the confirmed fraction from 88.0% to 69.2%, against 85.3% for the rule we use, which calls a tie unresolved (Methods). The undecided events are the smallest ones: at Ridgecrest the undecided share is 3% above M2.5 and 48% below M0.5 (Fig. S1e). The range is therefore widest for the catalogues that reach furthest below the completeness magnitude of the routine human-reviewed catalogue of the same region (e.g. the SCSN catalogue for Ridgecrest), which is exactly where a machine catalogue adds most of its events.

The four reviewers differ in how strict they are: their raw rates of events confirmed run from 50% to 91%, a spread of 41 points that would make the exercise look unreliable if taken at face value. However, they disagree about where to put the line and not about which events are better than which: all four put Kīlauea and Iquique at the top and ToC2ME last, and only the three catalogues in the middle change places between them (Fig. S1a). Because every reviewer judged every event, each reviewer's strictness can be estimated and removed. We fit a model in which each event carries a latent quality and each reviewer one threshold, its leniency, which is the observer's analogue of the station term that absorbs a site's systematic delay in earthquake location (Methods); one such term per reviewer, together with one quality per event, reproduces 89.5% of the 4,800 verdicts in sample (Table S5 and Fig. S1). That is a measure of fit and not of held-out prediction: on the most lenient reviewer the model does not beat an always-confirm baseline, because a reviewer who confirms 91% of what they see carries little to predict. In other words, the verdicts measure the catalogues, and the reviewers' personal thresholds are a nuisance that the crossed design removes.

The six catalogues are six different sequences, so the forty-point spread could come from the earthquakes or from the processing. The 2019 Ridgecrest sequence separates the two, because three independent catalogues of it exist over the same waveforms and the same stations: ours, the template-matching catalogue of Shelly (2020)[14] and the QTM catalogue of Ross et al. (2019)[4]. The sequence and the recordings are the same for all three, so any difference in what the panel confirms comes from how the catalogue was built. One reviewer judged a blind panel from each published catalogue, and the three were compared over the time and area they share, at matched magnitude and time since the mainshock (Methods). The Shelly catalogue is confirmed 92.5% of the time against 78.4% for QTM and 70.9% for ours, i.e. the catalogue we built ourselves is the one the panel stands behind least, a difference of 21.6 points, which clears the 13-point margin fixed before either new panel was reviewed (Note S9); it is also the most conservative of the three, holding 33,525 events in the shared window against 50,539 and 60,541. The difference lives entirely in the events each pipeline adds beyond the human-reviewed catalogue (Fig. 2c). On the events the human-reviewed catalogue also contains, the three pipelines agree (92% to 98% confirmed), whereas on their additions it is 88.3% for Shelly, 68.1% for ours and 60.4% for QTM. How much of a catalogue an expert can stand behind is therefore decided by the choices that built it and not by the sequence.

Reviewing every detection by a human seismologist in a catalogue of a million entries is out of the question, so the practical question is whether some quantity a catalogue already carries can stand in for the panel. The two substitutes in common use, a signal-to-noise threshold and agreement with another catalogue, both fall well below what the panel confirms at Ridgecrest (76.0% and 35.2% against 85.3%), and neither is calibrated, i.e. the confidence a rule implies for an event does not match how often such events are confirmed (Note S1).

A quantity that does reproduce the panel is what we call the ”confirmability” score, fitted at Ridgecrest to seven quantities that catalogue already records: phase count, station count, move-out residual, the two azimuthal gaps, nearest-station distance and magnitude. Under five-fold cross-validation it ranks an event the panel confirmed above one it rejected 94.6% of the time, over the 151 of 200 panel events the panel was willing to decide (AUC 0.946), and the probabilities it states track the fraction confirmed to within 0.04 once weighted back to the catalogue (Fig. S2a). Three of the six catalogues publish these association-stage quantities and can be scored from the catalogue alone; the other three publish no association record, and for them the equivalent features had to be measured from the waveforms (Note S5), so what the score needs is a property of what a catalogue chooses to release. It is not a restatement of event size, since magnitude alone separates confirmed from rejected at AUC 0.556 and removing magnitude from the model moves 0.946 only to 0.941. The events the panel could not decide are not invisible to the score: on the Ridgecrest panel the median score percentile is 13.5 for the events it rejected, 32.5 for the ones it left unresolved and 68.2 for the ones it confirmed, so the score places the unresolved population between the other two rather than mixing it into either. That matters for a tiered release, because the unresolved events are the small ones a machine catalogue exists to add. Used as a screen on the Ridgecrest catalogue, keeping the events whose confirmation probability is at least 0.7 retains 67.6% of the catalogue at a precision of 96% and a recall of 86% against the panel's verdicts (Fig. S2c).

The score also travels, as a ranking, although only one sequence lets us test it. Three of the six catalogues publish no association-stage record, so the Ridgecrest model cannot be applied to them at all, and at Iquique the panel rejected so few events that only one reviewer yields an estimate, whose interval reaches chance. That leaves the NE Japan forearc, where the Ridgecrest model applied unchanged orders three reviewers' own blind verdicts at AUC 0.73 to 0.79, against 0.93 within Ridgecrest itself (Fig. S2d, Fig. S3 and Table S4). What does not travel is the level: the score sits at a different height in each catalogue, so a threshold chosen at Ridgecrest neither keeps a comparable fraction nor delivers a comparable precision elsewhere. The ranking can therefore be transported while the level has to be re-anchored with a small blind panel, ~200 adjudications, in each new region; every ranking used below is fitted that way, on its own catalogue's panel (Methods).

The lowest-ranked events are not where the earthquakes are

The score ranks every event in a catalogue, and the panel's false verdicts fall at the bottom of that ranking, so the bottom is where we expect false detections to concentrate. Is there evidence of this in the catalogue itself, independent of the panel? Earthquakes occur on faults. The real events in a catalogue should therefore trace the fault structure of the sequence, whereas a false detection has no reason to fall systematically near a fault. If the lowest-ranked events sit further from the faults than the highest-ranked ones, or fail to form the planar structures that the highest-ranked ones form, that is evidence that they contain a larger share of false detections.

Fig. 3a puts the top and bottom thirds by score side by side for all six catalogues, matched in magnitude and depth so that neither third holds larger or deeper events than the other (Methods). At Ridgecrest the top third traces the conjugate strike-slip fault network while the bottom third fills the same volume as a diffuse cloud, the pattern repeats at Amatrice, in Japan and at Iquique, and the same contrast holds at depth (Fig. 3b).

To put a number on the maps we measured the distance from every event to the nearest fault, using a fault network fitted with the E2F method[16] to a random half of the Ridgecrest catalogue drawn without reference to the score (Methods). The median distance is nearly the same for the top and bottom thirds, but the bottom third has a tail of events far from every fault that the top third lacks (Fig. 3c): beyond 8 km lie 9% of the bottom third and none of the top. This is what a mixture predicts. Detections that no source produced have no reason to fall near a fault, whereas real events sit where real events sit whatever their score, so a contaminated population moves its tail and not its median; about a fifth of the bottom third at Ridgecrest lies more than 3 km from every fitted fault, against 0.4% of the top third (Fig. S5), and that fifth is the cloud in Fig. 3a. Location error is an unlikely explanation for the far tail, since the low-ranked events carry formal errors of 1 to 2 km, although those errors are the catalogue's own and have not been externally calibrated.

A second statistic needs no fault to be specified. The correlation dimension D_2 measures how a set of points fills space: it is close to 2 for events on a plane and close to 3 for events filling a volume (Fig. 3d). D_2 is measured on the top and bottom quartiles by score rather than the thirds used above, because the correlation integral needs the two groups well separated. At Ridgecrest the top quartile gives $D_2 = 2.30$ and the bottom quartile 2.81, so the high-ranked events lie close to planes and the low-ranked events fill the volume between them, and the same ordering holds in every catalogue where D_2 can be measured (Fig. S4 and Table S6).

Both contrasts could in part be produced by real events with poor locations, since a badly located real event also sits off its fault and also blurs a plane, and in a machine catalogue false detections and poor locations are entangled: the weak signals that produce one produce the other. Where the two can be separated, they answer differently. Among the events that the human-reviewed catalogue independently contains, which are real, most of the D_2 contrast remains but the off-fault tail vanishes (Figs S4c and S5c, and Methods). The far off-fault events are therefore machine-only detections, whereas most of the D_2 contrast is a matter of location quality.

The last test uses a tectonic structure whose form is known in advance: intraslab seismicity beneath NE Japan forms two sub-parallel planes ~30 km apart, the double seismic zone[17-18] (Fig. 4a). The top score quartile resolves both planes distinctly, whereas in the bottom quartile the lower plane is only a shoulder (Fig. 4b), and the difference persists at equal sample size, at matched depth and magnitude, and within latitude bands (Table S7). Location error is not sufficient to produce this: erasing the second plane requires about three times the depth error the bottom quartile actually carries (Fig. S6 and Note S4). The simpler reading is that a population diluted with false detections cannot resolve a structure its real members resolve.

Discussion

The high-ranked events are real and the low-ranked ones are a mixture

Taken together, our results support a simple reading. The events the confirmability score ranks high are real: they are the ones the panel confirms, they sit near faults, they lie on planes, and they resolve a known tectonic structure. The events it ranks low are a mixture in which false detections are common: they are the ones the panel declines, a fifth of them at Ridgecrest lie off every fault, they fill volume rather than planes, and they blur the double seismic zone. The panel's verdict on any one low-ranked event is nonetheless a bound and not a proof, since a magnitude –0.3 event recorded on six noisy channels may be real and still impossible to confirm by eye, which is why every such share in this paper is given as a range. What the panel measures is the fraction of a catalogue that expert review can stand behind. That is the quantity a user can act on, because a study that infers fault geometry, a b-value or a forecast inherits every detection in the catalogue and has no independent check on any of them.

The spread across the six catalogues, from 60% to 98%, has at least three causes mixed into it: the observing conditions, which place large events on dense networks at one end and ToC2ME's tiny events on a small array at the other; the association threshold, which sets how many marginal detections are admitted; and the detection threshold, which sets how far down the magnitude range a catalogue reaches. The last two are choices made by whoever built the catalogue, and the three-catalogue comparison at Ridgecrest shows that those choices alone move the confirmed fraction by ~20 points on the same sequence and the same waveforms. A single field-wide number for how much of a machine catalogue is real would therefore be meaningless. The confirmable fraction is a property of a particular catalogue built with particular settings, and it has to be measured per catalogue.

What a machine catalogue adds is selected, not sampled

The differences do not all live in the same place, and it is worth separating them. Two are confined to the events a machine catalogue adds beyond the human-reviewed catalogue: the three Ridgecrest pipelines agree to within a few points on the events that catalogue also contains and diverge only on their additions (88% of Shelly's confirmed against 60 to 68% for the other two), and the off-fault tail is absent from the reference-matched subset. Two are not so confined: three quarters of the correlation-dimension contrast survives among events that cannot be false, so it is largely a matter of how well an event can be located, and the double seismic zone was measured on a catalogue for which no human-reviewed reference is available to us, so the same control cannot be run there. What the added events have in common is that they are not a random sample of what the human-reviewed catalogue missed: they differ systematically in confirmation probability and in observational quality, and at Ridgecrest in where they sit relative to the faults. A machine catalogue is better described as a selective probabilistic measurement than as a list of earthquakes: it is selected on how observable an event was, observability is what the downstream analyses turn out to be sensitive to, and an analysis that treats all of its entries as equivalent inherits whatever selection produced them (Note S4).

Keeping a human anchor on machine-generated data

The wider problem this study is a case of has no obvious solution. AI systems now generate primary scientific data of every kind faster than anyone can check them, and the checking that does happen is usually internal, one model validated against another model's output or against a benchmark a third model assembled. Seismology is unusually well placed to resist this, and that is why we think the result travels. A detection is a claim about a waveform that still exists, which a trained person can adjudicate in about a minute; the scarce resource is therefore not the ability to verify but the number of verifications one can afford. What a calibrated, transferable score buys is leverage on that scarcity. In our case 4,800 human judgements were enough to place a defensible number on catalogues holding almost a million events between them and to rank every one of them, and about 200 adjudications in a new region are enough to re-anchor the level. The goal is neither to have humans check everything, which is impossible, nor to trust the machine, which is unfounded, but to maintain a live, quantified link between what the machine asserts and what a person is prepared to endorse, and to re-measure that link whenever the pipeline, the network or the region changes.

What follows for practice

Three things follow directly. Catalogues should be released tiered, with a score attached to each event and not as a single undifferentiated list; users doing structural work can take the high tier, users doing rate statistics can keep everything and weight, and nothing has to be deleted. A verification panel needs more than one reviewer, because a single reviewer's absolute level is displaced by their own leniency by tens of percentage points even when their ranking is sound. In addition, agreement with a reference catalogue should not be used as ground truth: it is biased low, it disagrees with itself depending on which reference is chosen, and it is redundant once waveform evidence is present (Note S1).

One cautionary note applies to the hours after a large mainshock. The features the score reads, i.e. phase count, station count and move-out residual, all degrade while the coda is busy, for reasons unrelated to confirmability, so a single threshold applied across a whole catalogue removes early aftershocks preferentially and distorts the aftershock decay: at Ridgecrest a global two-thirds cut moves the fitted Omori c from ~16 h to ~114 h, whereas the same cut applied within time windows leaves the decay where the human-reviewed catalogue puts it (Fig. S7). This is a problem of the early coda, where the detection threshold itself changes by the hour, and not of tiering in general. Immediately after a mainshock the tier should be set within time windows.

Methods

Catalogue construction

For Ridgecrest, Iquique and Hawai'i (Kīlauea) we built candidate catalogues from continuous waveforms. Three-component records were picked with PhaseNet[2] using the pretrained model without regional retraining, associated with PyOcto[20] and located with ADLoc. PyOcto was preferred to the Gaussian-mixture associator[21] for throughput on dense aftershock sequences. Association is the stage at which most spurious events are created; Note S2 describes a permutation test of the associator and why its result is not a false-discovery rate. For Amatrice, the NE Japan forearc and ToC2ME we audited published catalogues directly (Tan et al.[8], CAT5, 900,050 events; Suzuki et al.[9], 627,435 events; Igonin et al.[22], 18,040 events) and not reconstructions, so the audit applies to the products the community actually uses. Reported catalogue sizes are given per sequence in Table S1.

Auditing published catalogues instead of our own has a methodological cost we accept deliberately: the picking, association and location choices are not ours, so the audit measures the product and not our reproduction of it. That is the correct target.

Panel sampling

From each catalogue we drew a stratified sample of 200 events. For Ridgecrest the strata are the 24 cells of a $3 \times 4 \times 2$ grid: associated phase count (8–14, 15–24, $\geq$25), magnitude (<0.5, 0.5–1.5, 1.5–2.5, $\geq$2.5), and whether the event matches an independent high-resolution catalogue. The other sequences follow the same principle on different variables, because the catalogues record different things: Iquique on phase count, depth and external support; Amatrice on magnitude, location quality and support; ToC2ME on magnitude, injection stage, depth and support; Kīlauea on magnitude, time and support. All are listed in Table S2.

Stratification is deliberately disproportionate: rare cells that carry large population weight are oversampled relative to their frequency, which is what makes a 200-event panel informative about a catalogue that may be thousands of times larger. Population estimates are therefore design-weighted, with each sampled event carrying weight equal to the inverse of its stratum's sampling fraction. Confidence intervals are computed by stratified bootstrap over 10,000 resamples drawn within strata.

The estimator is the ratio of two design-weighted totals: the weighted share of the catalogue judged confirmed, divided by the weighted share judged either confirmed or rejected. It is not a weighted mean of the within-stratum precisions, which is a different quantity and does not decompose against the class shares reported beside it.

A stratum carrying large population weight but few adjudicated events contributes a high-variance ratio at high weight, so a partially filled panel gives an unstable estimate. The blind panel is not in that regime: all

24 Ridgecrest strata carry at least six adjudicated events, and no stratum with fewer than five verdicts holds any weight. What a partially filled version of the same design does, and why the instability is a property of the estimator and not of the reviewers, is set out in Note S7.

Panel design

The panel was designed around a two-reviewer agreement gate declared before the verdicts were read. That gate failed, and the disagreement it detected was a difference in threshold between reviewers rather than noise, so the design was changed to four reviewers each judging all 200 events of every sequence, fully crossed, which identifies that difference and removes it (Note S7).

Blinding and the review interface

Each sampled event was rendered as a record section of the five nearest stations with data that day, band-passed at 2 to 15 Hz, sorted by epicentral distance, each trace normalised to its own maximum, with the predicted P and S from a straight-ray 6.0 km s^{-1} model drawn on every row. The six sequence panels show all three components over a $\pm$20 s window; the two further Ridgecrest panels show the vertical component alone over –2 to +12 s, with the channel code printed, because the first pass on those panels left the component ambiguous and was discarded (below). No catalogue metadata reaches the image: the panel is drawn without an origin time, a latitude, a longitude, a depth, a magnitude, a station name or a station distance, and the rows carry only their rank in distance, since five distances against a known network would locate the event. The identical image file was then shown to every reviewer, so differences between reviewers cannot arise from differences in the stimulus. Verdicts recorded through any earlier interface are not used. Figure 1 is redrawn from three of these images: it carries the same waveforms, the same station selection, the same predictions and the same blinding, although it shows the vertical component over a shorter window for legibility where the portal drew all three components over $\pm$20 s. It adds nothing the reviewer did not have, and the images themselves are in the archive.

Combining four verdicts into one label

Every event on the blind panel carries four independent verdicts drawn from {rejected, unresolved, confirmed}. The panel label is their plurality, with ties resolved to unresolved. The rule is implemented once and imported by every product that needs a label (the precision estimate, the calibration curves and the retention tiers), so that no two results in this paper rest on different definitions of the same quantity.

Ties matter: 22 of the 200 events split two against two, and the convention chosen for them moves the design-weighted precision from 69.2% (ties counted rejected) to 88.0% (ties counted confirmed), with 85.3% for the rule we use. Calling them unresolved is what a two-two split means, and it leaves the ambiguity where it is visible, in the partial-identification bracket, instead of resolving it silently. Everything that depends on a binary label (AUC, calibration, tiers) is computed on the 151 events the panel resolved; the 49 it did not are excluded from those quantities and retained in the bracket.

Two models, and what each is for

One quantity, the confirmability score, is attached to every event in every catalogue, and it is fitted in two ways that answer different questions, so we state at the outset which is which. On all six sequence catalogues it is a ridge regression on the panel's latent event quality and is used as a ranking; at Ridgecrest, where the panel resolved a confirmed-against-rejected label, it is refitted as a logistic regression and its value is then a calibrated confirmation probability. The two fits share their features and agree in ordering; only the second carries a number that means a probability.

The confirmability score as a ranking. On all six catalogues, wherever a ranking is needed (the transfer test, the correlation dimension, the double seismic zone) the score is a ridge regression on the latent event quality θ of the leniency model, with the penalty chosen by cross-validation and performance reported as the out-of-fold rank correlation with θ (Note S6). Regressing on θ rather than on a thresholded label is what lets one method serve all six sequences, three of which will not support a binary classifier at all: the Kīlauea panel resolves 185 confirmed against only 5 rejected, ToC2ME's quantised origin times leave the move-out feature missing for most events, and Amatrice's published catalogue carries no association-stage record. For those three the ranking is the only score we report.

Two feature families exist across the six catalogues. Ridgecrest, Iquique and the NE Japan forearc distribute association-stage quantities (phase and station counts, move-out residual, azimuthal gaps, station distance, magnitude). Amatrice, ToC2ME and Kīlauea required the waveforms to be re-read for signal-to-noise. The transfer test therefore trains on Ridgecrest's association features and applies that model unchanged to the two other catalogues carrying them, scored against each reviewer's own blind verdicts. An AUC is reported only where that reviewer rejected at least ten events, otherwise the negative class is too small for the statistic to mean anything; three reviewers pass that bar in the NE Japan forearc and one at Iquique, so the Iquique transfer is untested more than failed (Table S4). Where the families differ the model is fitted on that catalogue's own panel, and we describe it as such and not as one model.

The confirmability score as a probability, at Ridgecrest. Wherever a number has to mean a probability (the reliability diagram, the model-variant comparison and the retention tiers of Fig. S2a–d) the model is an ℓ_2-regularised logistic regression on the binary panel label, confirmed against rejected, with the events the panel left unresolved excluded, fitted at a fixed penalty on features standardised within each training fold (Note S6). Calibration is summarised by the expected calibration error, the population-weighted average gap between the probability the model states and the fraction of such events the panel confirmed. We report all four binning and weighting combinations in Note S6 and quote the most conservative, 0.040. Platt scaling[23] was tried and is not used: it leaves the error slightly worse, at 0.025 against 0.018 on the panel, because the raw score is already close to calibrated.

Waveform features

Signal-to-noise ratios are measured as the ratio of root-mean-square amplitude in a signal window after the predicted P arrival to that in a preceding noise window, in a band fixed across the region and in a band adapted to the source corner frequency[24], the attenuation cutoff[25] and the instrument. **The move-out residual** is the root-mean-square misfit between the observed picks and the arrival times a 1-D velocity model predicts from the candidate hypocentre, over the stations passing a signal-to-noise gate. **Station support** counts the channels above fixed thresholds. Windows, passbands, velocity models and gates are set per catalogue, because a catalogue that quantises its origin times to 1 s cannot be measured with the windows that suit one resolved to 0.01 s; every value, and the sensitivity of the ToC2ME ranking to the one instrument corner we could not verify, is given in Note S5.

Estimands and validation

Both fits of the confirmability score use the same seven features listed in Results: phase count, station count, the move-out residual, primary and secondary azimuthal gap, distance to the nearest station, and magnitude. The waveform quantities described above enter only the three sequences whose catalogues carry no association-stage record.

The bracket. Because the reviewers were free to decline, the population confirmed share is bounded and not point-identified. The bounds are obtained by assigning the entire unresolved class to one side and then the other, and re-running the same design-weighted estimator: assigning all of it to rejected gives the lower bound, all of it to confirmed the upper. The ends of that ordering are stable under every convention for the undecided events, with Kīlauea and Iquique highest and ToC2ME lowest, but the middle is not: the NE Japan forearc ranks third when the undecided are counted as rejected and fifth when they are counted as confirmed. No distributional assumption is made about the unresolved events, which is the point, since the width of the bracket is the price of not making one. The design weights are very uneven, and in the Japan forearc a single adjudicated event stands for 4,259 catalogue events, so we also asked whether any one cell carries the estimate. Refitting with each stratum dropped in turn moves the estimate by at most 4.1 points anywhere in the six sequences, and dropping any single adjudicated event moves it by at most 1.3 points, both well inside the confidence intervals. The events the panel left unresolved are excluded from the classifier entirely instead of recoded into it, so no model in this paper depends on a convention for them; the bracket carries that ambiguity instead.

Cross-validation. Both models are validated by five-fold cross-validation, stratified on the label for the binary model and unstratified for the ridge fit, whose target is continuous.

Reviewer leniency

Reviewer r facing event e is modelled as responding to a latent endorsability

$$z_{er} = \theta_e - b_r + \varepsilon_{er}, \qquad \varepsilon_{er} \sim \text{Logistic}(0, 1),$$

which two global cut points $c_1 < c_2$ divide into the three verdicts. Writing $\sigma(x) = (1 + e^{-x})^{-1}$ for the logistic function, the probability of each verdict is

$$\begin{aligned}
\Pr(\text{rejected} \mid e, r) &= \sigma(c_1 - \theta_e + b_r)\,, \\
\Pr(\text{unresolved} \mid e, r) &= \sigma(c_2 - \theta_e + b_r) - \sigma(c_1 - \theta_e + b_r)\,, \\
\Pr(\text{confirmed} \mid e, r) &= 1 - \sigma(c_2 - \theta_e + b_r)\,.
\end{aligned}$$

Here θ_e is the event's quality on a scale common to all regions and b_r is the reviewer's leniency, exactly as a station term absorbs a site's systematic delay in relocation. A strict reviewer carries a large positive b_r and requires more evidence to say confirmed; the two enter only through the difference $\theta_e - b_r$, which is what makes the separation possible at all.

Identification comes from overlap: reviewers judge the same fixed 200-event panels, and we impose $\sum_r b_r = 0$ with shared cut points $c_1 = -1, c_2 = +1$. A reviewer who never overlapped anyone would not be separable from the events they saw. The parameters maximise the log-likelihood

$$\ell(\boldsymbol{\theta}, \mathbf{b}) = \sum_{(e,r)\in\mathcal{O}} \log \Pr(v_{er} \mid e, r),$$

over the set $\mathcal{O}$ of observed event-reviewer pairs, where v_{er} is the verdict recorded. Because θ_e enters only the terms for event e, the model is fitted by profiling, alternating a per-event 1-D solve with a per-reviewer 1-D solve, which converged in 14 iterations on 4,800 verdicts over 1,200 events and reproduces 89.5% of individual verdicts.

Two limitations are worth stating. Under leave-one-out the model does not beat an always-confirm baseline for the most lenient reviewer (90.0% versus 90.9%), although it beats that baseline by 7 to 15 points on the other three, because a reviewer who calls 91% of events confirmed carries little information to predict. In addition, θ is bounded at ± 8 in the fit, and 46% of the 1,200 events sit at the upper bound; these are the events all four reviewers confirmed, among which the panel supplies no ordering. The confirmability score is therefore fitted to a target that is flat over the best half of every panel, and its rank correlation with θ (+0.44 to +0.75 by catalogue, Table S8) should be read with that ceiling in mind, and in particular the ordering the score imposes inside the top tier is not something the panel can corroborate; the binary comparisons at Ridgecrest are unaffected.

Correlation dimension

D_2 is estimated by the Grassberger–Procaccia[27] method. Hypocentres are projected to a local Cartesian frame in kilometres, and for N events at positions $\mathbf{x}_i$ the correlation integral counts the pairs closer together than r,

$$C(r) = \frac{2}{N(N-1)} \sum_{i<j} H(r - \|\mathbf{x}_i - \mathbf{x}_j\|) \,,$$

with H the Heaviside step. Where the hypocentres are self-similar, $C(r) \propto r^{D_2}$, so the exponent is the slope of the log–log curve,

$$D_2 = \frac{\mathrm{d}\log C(r)}{\mathrm{d}\log r},$$

fitted by least squares on 14 logarithmically spaced radii. Two separate thresholds are involved and they are not the same number. The usable range is first measured per catalogue on a 60-radius scan, as the widest interval over which $10^{-4} < C(r) < 10^{-1}$; this is deliberately conservative, since it is what decides whether a catalogue is reported at all. The slope is then fitted inside that range over the radii where $10^{-6} < C(r) < 0.4$, which drops only the empty and saturated ends of the fitting window itself. D_2 is declined outright where the usable range spans less than one decade in r, the criterion that excludes ToC2ME (0.46 decades) and Kīlauea (0.97). Measuring the window per catalogue instead of fixing one across regions matters more than it looks (Fig. S4). High- and low-score groups are compared at equal sample size, because the correlation integral depends on how many points fall in the box: each group is drawn without replacement to the smaller of the two, capped at 8,000 events, over 20 draws. Where a group is small enough that the cap does not bind, the draw is held to 90% of it, so that repeated draws are not the same set in a different order and the reported spread stays meaningful.

Network geometry is not removed from the score before D_2 is computed, because the station count and the azimuthal gaps record how clearly an event announced itself and not only how well the network could have seen it; residualising on them removes evidence along with the confounder, and those residualised contrasts are reported in Fig. S4a as a deliberately over-strong floor (Note S8). The control that addresses location quality without removing evidence is the reference control below.

Fault-segment fitting

E2F[16] is applied through a Python port of the released MATLAB implementation, validated against the ToC2ME example distributed with it: at the published control scale the largest fault holds 4,490 events against the published 4,489, and its strike and dip agree to the reported precision. The pipeline is unchanged. A three-dimensional Hough transform assigns events to linear and planar trends, an iterative DBSCAN then cuts each trend into segments with $\epsilon = C\,R(M_w)$, where R is the magnitude-derived radius of the original and M_w the largest magnitude remaining in the trend, and a PCA ellipsoid is fitted to each segment of at least six events.

Neither of E2F's two length scales carries a default that travels between sequences, so both are set per catalogue by a scan and chosen on the count of segments holding at least fifty events whose planarity lies in [0.8, 1]. The released selection metric is not used unmodified, because its scalar-moment criterion accepts every segment in all six of our catalogues and therefore only rewards fragmentation. The scan, the chosen scales, the fifty-event floor and its robustness are given in Note S8 and Tables S10 and S11. Groups within a catalogue are drawn to a common magnitude histogram, and five random draws to the same histogram give the null. Location precision is not removed from the score either; the control applied is the reference control described below, which needs no error model.

Double seismic zone

Events are restricted to depth ≥ 60 km and to distances within [–20, +70] km of the Slab2[19] interface, where the sign convention is positive below the interface. This catalogue is scored with the confirmability score as a ranking and not as a calibrated probability, so groups are defined by percentile of the fitted score $\hat{\theta}$: the top quartile ($\hat{\theta} \geq 6.94$) against the bottom quartile ($\hat{\theta} \leq 4.28$), with both thresholds reported. The split is symmetric and the result does not depend on it; a sweep from bottom-decile-against-top-quartile to a median split is given in Table S7.

The primary statistic is how far apart the two planes sit relative to their own width. Fitting a two-component Gaussian mixture to the distances below the interface gives means $\mu_1 < \mu_2$, standard deviations σ_1, σ_2 and weights w_1, w_2, and the separation ratio is

$$S = \frac{\mu_2 - \mu_1}{\sqrt{w_1\sigma_1^2 + w_2\sigma_2^2}}.$$

No smoothing parameter enters it. Groups are equalised by subsampling, and the spread is taken over 40 draws at 80% of the smaller group's size, because drawing the full group without replacement would give every draw the same set and a spread of exactly zero.

Two further summaries, a kernel-density mode count and a Bayesian information criterion[28] comparison of a two-component against a one-component mixture, are reported in Note S8, and neither is used to separate the groups. Two spatial controls are applied: the high-confirmability group is drawn to the low-confirmability group's own depth histogram, and the comparison is repeated within one-degree latitude bands (Note S8).

Slab2 enters only as a common reference surface: both groups are measured against the same surface at the same depth, so the contrast is insensitive to its absolute accuracy. It is not accurate enough to support a claim about how the plane separation varies with depth, and we make none (Note S3). The fitted spacing of the two planes is 30.3 km, and the separation ratio is 3.25 (95% CI 3.23 to 3.29) in the top quartile against 2.86 (2.82 to 2.91) in the bottom, a difference of +0.39 (+0.34 to +0.45).

Three catalogues of one sequence

Every catalogue audited above is a different sequence, so a difference in confirmed fraction between two of them could come from the earthquake sequence or from the processing. The 2019 Ridgecrest sequence is the one case where that can be separated, because three independent catalogues of it exist over the same continuous waveforms and the same stations: our PhaseNet, PyOcto and ADLoc catalogue; the catalogue of Shelly (2020)[14], built by matched-filter detection against routinely catalogued events and relative relocation (34,091 events, 4 to 16 July 2019); and the QTM catalogue of Ross et al. (2019)[4], built by matched-filter detection at the 9$\times$ median-absolute-deviation threshold of the QTM method[15] and relocated with GrowClust (111,918 events, distributed by the Southern California Earthquake Data Center). We audited the two published catalogues as distributed. Two of the three are template-matching catalogues, so the contrast is not between algorithm families. Within the common support the three hold 33,525 (Shelly), 50,539 (ours) and 60,541 (QTM) events, with completeness magnitudes of 0.95, 0.85 and 0.45, respectively, so the most conservative catalogue is the cleanest; whether that follows from its detection threshold or from its requirement that an event relocate successfully cannot be separated with these two catalogues alone.

From each of the two published catalogues we drew a stratified panel of 200 events on the variables that catalogue records, rendered them under the same blinding rules as the six original panels, and had one of the four original reviewers judge them through the same portal. The comparison is restricted to the time and space the three panels share, and because the arms differ in magnitude and in time since the mainshock, the confirmed fraction is estimated from a logistic model with terms for pipeline, magnitude and log time, standardised to the pooled covariate distribution, with intervals from 600 bootstrap resamples drawn within arm. The decision rule, including a substantive margin of 13 percentage points, was fixed and committed before either panel was reviewed, and is set out in full in Note S9. The panels, the covariate handling, the pre-registered rule and the one gate it trips are set out in Note S9.

Whether the human-reviewed catalogue independently contains an event is decided by matching to the SCSN/ComCat catalogue for 4 July to 4 August 2019 within 3 s in origin time and 5 km in epicentre. The split of Fig. 2c is descriptive, with Jeffreys 95% intervals on the confirmed fraction among decided events.

Matched thirds for the maps

The map and section views of Fig. 3a,b compare the top and bottom thirds of each catalogue by confirmability score. A visible difference in how tightly the two sit is only a difference in organisation if the two thirds occupy the same part of the catalogue in every other respect. Both are therefore drawn to a common joint histogram in magnitude (0.2-unit bins) and depth (2 km bins, or 10 km for the forearc slab) before plotting, by taking in each cell the smaller of the two counts and sampling that many from each third. Beneath NE Japan the high-ranked events are deeper on average than the low-ranked ones, since a crustal event at a given magnitude is recorded against more noise than an intraslab one, and an unmatched pair of maps reads that depth difference as a difference in footprint. The bottom third is also smaller on average, because magnitude is one of the score's features, which is why the matching is done; its frequency–magnitude distribution is nonetheless close to Gutenberg–Richter at Ridgecrest and Amatrice (Fig. S8), so the low-ranked population could not have been isolated from the magnitudes alone. Frames are the joint 2nd to 98th percentile extent, cropped along the longer axis about the median of the seismicity so that every panel is filled.

The off-fault tail, and the reference control

The distance from each held-out event to the nearest fitted fault segment is computed as described under fault-segment fitting, against a network fitted once to a random half of the catalogue drawn without reference to the score. The statistic kept in the main text is not the median of that distance but the fraction of each third that lies further than a given distance from every fitted segment, because it is the statistic a mixture predicts. The false detections in a third have no reason to fall near a fault, whereas the real events in the same third sit where real events sit, so the median barely moves and the whole effect is in the far tail. Ratios between the thirds are given with bootstrap intervals; where the top third contains no event beyond a threshold the ratio is undefined and is reported as counts, not as a large number.

Two confounders are removed before the tail is read, since reference-matched events are systematically larger than the catalogue as a whole and whether an event reached the regional catalogue depends on when it happened; every comparison involving them is therefore made inside a common magnitude window and beyond 24 h after the mainshock (Note S10).

The reference control removes confirmability as an explanation by construction. Restricting to the detections the human-reviewed regional catalogue independently contains, none of which can be false, and repeating the score split inside that subset asks whether the contrast can be produced without any false detection at all; the reading was fixed before the result was computed. For the correlation dimension 75% of the Ridgecrest contrast survives the control (+0.37 against +0.50), so D_2 is presented as evidence that catalogue quality structures a geometric statistic and not as evidence of contamination. For the fault distance 17% survives (+0.07 km against +0.41 km) and the fraction beyond 10 km falls from 6.7% to 0.4%, so the tail is concentrated in detections the human-reviewed catalogue does not contain. Whether those are false can only be tested against the panel's own verdicts, and at 200 events that test is a null with a standard error of 0.11 in $\log_{10}$ distance against a full-catalogue effect of about 0.15, which is a statement about power and not about absence. The controls, the widened match radius and the verdict-linked regression are given in Note S10.

Aftershock decay under tiering

The cost of tiering on the time axis is measured against the SCSN/ComCat catalogue with the modified Omori law, n(t) = K (t + c)^–p, fitted by maximum likelihood with c free over 1 h to 28 days after the M7.1, for events above M1.5. Six selections are compared: the human-reviewed catalogue; the flat machine catalogue; the machine catalogue keeping the top two thirds by one global score threshold; and the machine catalogue keeping the top two thirds within each of six, eight or twelve logarithmically spaced time windows. A straight-line fit through log-spaced count bins, the estimator often used for a quick look, has no c and returns exponents near 0.65 for this sequence, whose published value is close to 1.1; the maximum-likelihood fit gives 1.10 for the human-reviewed catalogue and is the one reported. A global threshold moves c from ~16 h to ~114 h and p from 1.10 to 1.52, because the fit has to explain a missing early population; the within-window thresholds leave both where the human-reviewed catalogue puts them (Fig. S7).

Limitations

Four limits bound what we claim. The four reviewers are authors, so the ground truth is the author team's opinion under blinding and not an independent one. The panels are 200 events each and cannot resolve small verdict-linked differences in geometry, which is why the off-fault tail is attributed to machine-only detections and not to false ones. The three-catalogue comparison rests on one sequence, one reviewer for the two published catalogues, and a magnitude trim that removes a third of our own panel. In addition, the score transfers as a ranking to one of the two sequences where it could be tested and is uninformative in the other. What would settle the largest of these is independent confirmation of the specific detections the panel declined, e.g. a dense array over part of the same sequence, and building two catalogues from the same continuous data with the same detector at two admission thresholds would separate the threshold from the method in the three-catalogue result.

Data availability

All data required to reproduce the results are public, at doi:10.5281/zenodo.22059219, under CC BY 4.0. The deposition holds the blinded panel images shown to reviewers, the verdict tables under the reviewer labels R1–R4, whose mapping to the four authors is given in Table S5, the single-reviewer verdicts on the two further Ridgecrest panels together with the quarantined first pass on them, the confirmability-scored catalogues for all six sequences, the waveform feature tables, and the derived products behind every figure and table.

Independent reference catalogues used for stratification and for the comparisons in Note S1 are the template-matched Ridgecrest catalogue[4] and the SCSN analyst catalogue for Ridgecrest, and the double-difference relocated forearc catalogue[6] and the Iquique sequence catalogue[7] for northern Chile.

The candidate catalogues audited here are the authors' own or are publicly distributed: Amatrice CAT5 (doi:10.5281/zenodo.4736089), the NE Japan forearc catalogue (doi:10.5281/zenodo.13854225) and the ToC2ME beamforming catalogue (doi:10.1029/2020JB020311). Source waveforms are available from the Southern California Earthquake Data Center, GFZ Potsdam, EIDA/INGV, EarthScope, NIED Hi-net and

S-net, and the U.S. Geological Survey.

The four adjudicators are the four authors, identified in Table S5; individual verdicts are released under the labels R1–R4.

Code availability

All analysis code, including the scripts that generate every figure and every table in the Supplementary Information, is in the same public deposition, doi:10.5281/zenodo.22059219. The archive also contains a test that checks every headline number in the manuscript, the Supplementary Information and the figure captions against its source data product.

Acknowledgements

This work was supported by U.S. National Science Foundation award EAR-2506181. We thank the operators of the seismic networks whose continuous data made this audit possible: the Southern California Earthquake Data Center, GFZ Potsdam, EIDA and INGV, EarthScope, NIED (Hi-net and S-net), and the U.S. Geological Survey. We thank the authors of the published catalogues audited here, in particular Y. J. Tan and colleagues, W. Suzuki and colleagues, N. Igonin and colleagues, D. R. Shelly, and Z. E. Ross and colleagues, for distributing their products openly, which is what made an independent audit possible at all.

Author contributions

L.M. conceived the study, designed the audit, and wrote the manuscript. L.M., H.H., J.M. and Y.M. each performed the blind waveform adjudication of all six sequence panels and validated the results; L.M. additionally adjudicated the two further Ridgecrest panels used in the three-catalogue comparison. All authors reviewed and edited the manuscript.

Competing interests

The authors declare no competing interests.

Use of AI

Anthropic's Claude was used as a coding and analysis assistant throughout this project. It implemented and executed the processing, scoring and statistical code, prepared documentation, surveyed literature, and assisted in preparing manuscript text. The scientific content is the authors' own, and the manuscript was written or rewritten, edited and approved by the authors. All figures are hand-authored vector graphics generated by the analysis code; no figure, schematic or illustration was produced by a generative image model. All scientific questions, study design decisions and interpretations are the authors'. Every one of the 4,800 waveform verdicts reported here was made by a named human author; none was generated by AI. The authors verified the analyses and take full responsibility for the content.

References

1. Mousavi, S. M. & Beroza, G. C. Machine learning in earthquake seismology. *Annu. Rev. Earth Planet. Sci.* **51**, 105–129 (2023). doi:10.1146/annurev-earth-071822-100323

2. Zhu, W. & Beroza, G. C. PhaseNet: a deep-neural-network-based seismic arrival-time picking method. *Geophys. J. Int.* **216**, 261–273 (2019). doi:10.1093/gji/ggy423
3. Mousavi, S. M., Ellsworth, W. L., Zhu, W., Chuang, L. Y. & Beroza, G. C. Earthquake transformer — an attentive deep-learning model for simultaneous earthquake detection and phase picking. *Nat. Commun.* **11**, 3952 (2020). doi:10.1038/s41467-020-17591-w
4. Ross, Z. E. et al. Hierarchical interlocked orthogonal faulting in the 2019 Ridgecrest earthquake sequence. *Science* **366**, 346–351 (2019). doi:10.1126/science.aaz0109
5. Shelly, D. R. & Thelen, W. A. Anatomy of a caldera collapse: Kīlauea 2018 summit seismicity sequence in high resolution. *Geophys. Res. Lett.* **46**, 14395–14403 (2019). doi:10.1029/2019GL085636
6. Sippl, C., Schurr, B., Asch, G. & Kummerow, J. Seismicity structure of the northern Chile forearc from >100,000 double-difference relocated hypocenters. *J. Geophys. Res. Solid Earth* **123**, 4063–4087 (2018). doi:10.1002/2017JB015384
7. Soto, H. et al. Probing the northern Chile megathrust with seismicity: the 2014 M8.1 Iquique earthquake sequence. *J. Geophys. Res. Solid Earth* **124**, 12935–12954 (2019). doi:10.1029/2019JB017794
8. Tan, Y. J. et al. Machine-learning-based high-resolution earthquake catalog reveals how complex fault structures were activated during the 2016–2017 Central Italy sequence. *Seismic Record* **1**, 11–19 (2021). doi:10.1785/0320210001
9. Suzuki, W. et al. The forearc seismic belt: a fluid pathway constraining down-dip megathrust earthquake rupture. *Science* **389**, 190–194 (2025). doi:10.1126/science.adt6389
10. Beroza, G. C., Segou, M. & Mousavi, S. M. Machine learning and earthquake forecasting — next steps. *Nat. Commun.* **12**, 4761 (2021). doi:10.1038/s41467-021-24952-6
11. Mancini, S., Segou, M., Werner, M. J. & Parsons, T. On the use of high-resolution and deep-learning seismic catalogs for short-term earthquake forecasts. *J. Geophys. Res. Solid Earth* **127**, e2022JB025202 (2022). doi:10.1029/2022JB025202
12. Noel, S. K. & West, M. E. Challenges and opportunities of machine learning earthquake detection for regional monitoring. *Bull. Seismol. Soc. Am.* **115**, 2096–2108 (2025). doi:10.1785/0120250016
13. Herrmann, M. & Marzocchi, W. Inconsistencies and lurking pitfalls in the magnitude–frequency distribution of high-resolution earthquake catalogs. *Seismol. Res. Lett.* **92**, 909–922 (2021). doi:10.1785/0220200337
14. Shelly, D. R. A high-resolution seismic catalog for the initial 2019 Ridgecrest earthquake sequence: foreshocks, aftershocks, and faulting complexity. *Seismol. Res. Lett.* **91**, 1971–1978 (2020). doi:10.1785/0220190309
15. Ross, Z. E., Trugman, D. T., Hauksson, E. & Shearer, P. M. Searching for hidden earthquakes in Southern California. *Science* **364**, 767–771 (2019). doi:10.1126/science.aaw6888
16. He, Z. & Wang, R. E2F: extract fault geometry from earthquake catalogs. *Seismol. Res. Lett.*(2025). doi:10.1785/0220250138 17. Umino, N. & Hasegawa, A. On the two-layered structure of deep seismic plane in northeastern Japan arc.*Zisin* **28**, 125–139 (1975).
17. Hasegawa, A., Umino, N. & Takagi, A. Double-planed structure of the deep seismic zone in the northeastern Japan arc. *Tectonophysics* **47**, 43–58 (1978).
18. Hayes, G. P. et al. Slab2, a comprehensive subduction zone geometry model. *Science* **362**, 58–61 (2018). doi:10.1126/science.aat4723

19. Münchmeyer, J. PyOcto: a high-throughput seismic phase associator. *Seismica* **3** (2024). doi:10.26443/seismica.v3i1.1130

20. Zhu, W., McBrearty, I. W., Mousavi, S. M., Ellsworth, W. L. & Beroza, G. C. Earthquake phase association using a Bayesian Gaussian mixture model. *J. Geophys. Res. Solid Earth* **127**, e2021JB023249 (2022). doi:10.1029/2021JB023249

21. Igonin, N., Verdon, J. P., Kendall, J.-M. & Eaton, D. W. Large-scale fracture systems are permeable pathways for fault activation during hydraulic fracturing. *J. Geophys. Res. Solid Earth* **126**, e2020JB020311 (2021). doi:10.1029/2020JB020311

22. Platt, J. Probabilistic outputs for support vector machines and comparisons to regularized likelihood methods. In *Advances in Large Margin Classifiers* 61–74 (MIT Press, 1999).

23. Madariaga, R. Dynamics of an expanding circular fault. *Bull. Seismol. Soc. Am.* **66**, 639–666 (1976).

24. Anderson, J. G. & Hough, S. E. A model for the shape of the Fourier amplitude spectrum of acceleration at high frequencies. *Bull. Seismol. Soc. Am.* **74**, 1969–1993 (1984).

25. Uchida, N., Nakajima, J., Wang, K. et al. Stagnant forearc mantle wedge inferred from mapping of shear-wave anisotropy using S-net seafloor seismometers. *Nat. Commun.* **11**, 5676 (2020). doi:10.1038/s41467-020-19541-y

26. Grassberger, P. & Procaccia, I. Measuring the strangeness of strange attractors. *Physica D* **9**, 189–208 (1983).

27. Schwarz, G. Estimating the dimension of a model. *Ann. Stat.* **6**, 461–464 (1978).

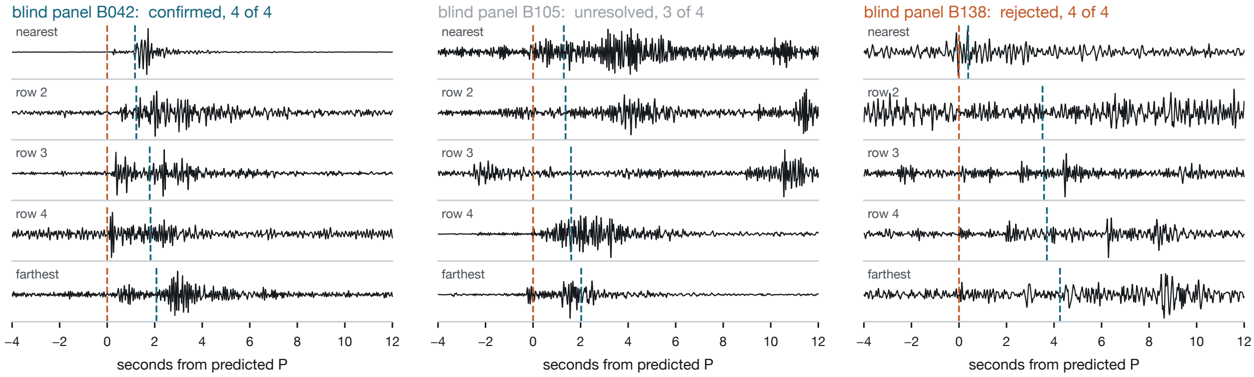

Fig. 1 | What a reviewer saw. Three entries from the Ridgecrest panel, with the verdict the four reviewers returned on each. Each is a record section of the five nearest stations, ordered from nearest (top) to farthest (bottom) and identified only by that rank; time runs from the P arrival predicted for that station, marked in red, and the blue line marks the predicted S. Nothing the catalogue asserts about the event is shown, and Methods gives the display and the blinding in full. Left, an entry all four reviewers confirmed: an impulsive onset at the predicted P on every row, with an S that arrives progressively later, which is the move-out a real source produces. Centre, an entry three of four left unresolved: an onset is present on the farther rows, although on the nearest ones it is overprinted by a larger event a few seconds later. Right, an entry all four rejected: the catalogue lists it at magnitude 2.6, and no row carries a coherent arrival at the prediction. The unresolved category is kept throughout, which is why every confirmed fraction is reported with a range.

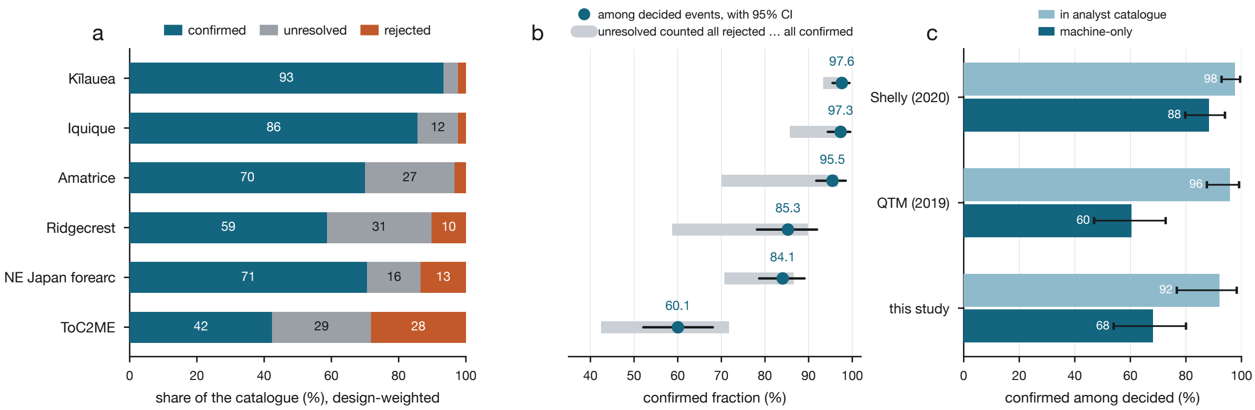

Fig. 2 | How much of each catalogue the panel stands behind, and whether that depends on the sequence or on the pipeline. **a**, The panel's verdict on each of the six sequence catalogues, four reviewers combined by plurality into confirmed, unresolved or rejected. Bars are design-weighted, so they describe the catalogue and not the panel (Methods). **b**, The number a user can act on. The dot is the confirmed fraction among decided events with its 95% confidence interval; the grey bar is the range that results from assigning every unresolved event first to rejected and then to confirmed, and the paper reports that bracket rather than choosing a convention. **c**, The same sequence in three catalogues. Three independent catalogues of the 2019 Ridgecrest sequence, built from the same waveforms and the same stations by different pipelines, were each sampled and judged blind over the time and area the three share. The labels are not identical across the arms: ours carries the four-reviewer panel consensus, the two published catalogues carry the verdicts of one of those four reviewers, who judged them through the same portal. The adjusted contrasts quoted in the Results are computed on that reviewer's own verdicts in all three arms, which is the like-for-like construction (Note S9). Bars give the confirmed fraction among decided events with Jeffreys 95% intervals, split by whether the human-reviewed regional catalogue independently contains the event (light) or does not (dark). The three pipelines agree on the events the human-reviewed catalogue also holds, and differ by up to 28 points on the events each adds beyond it.

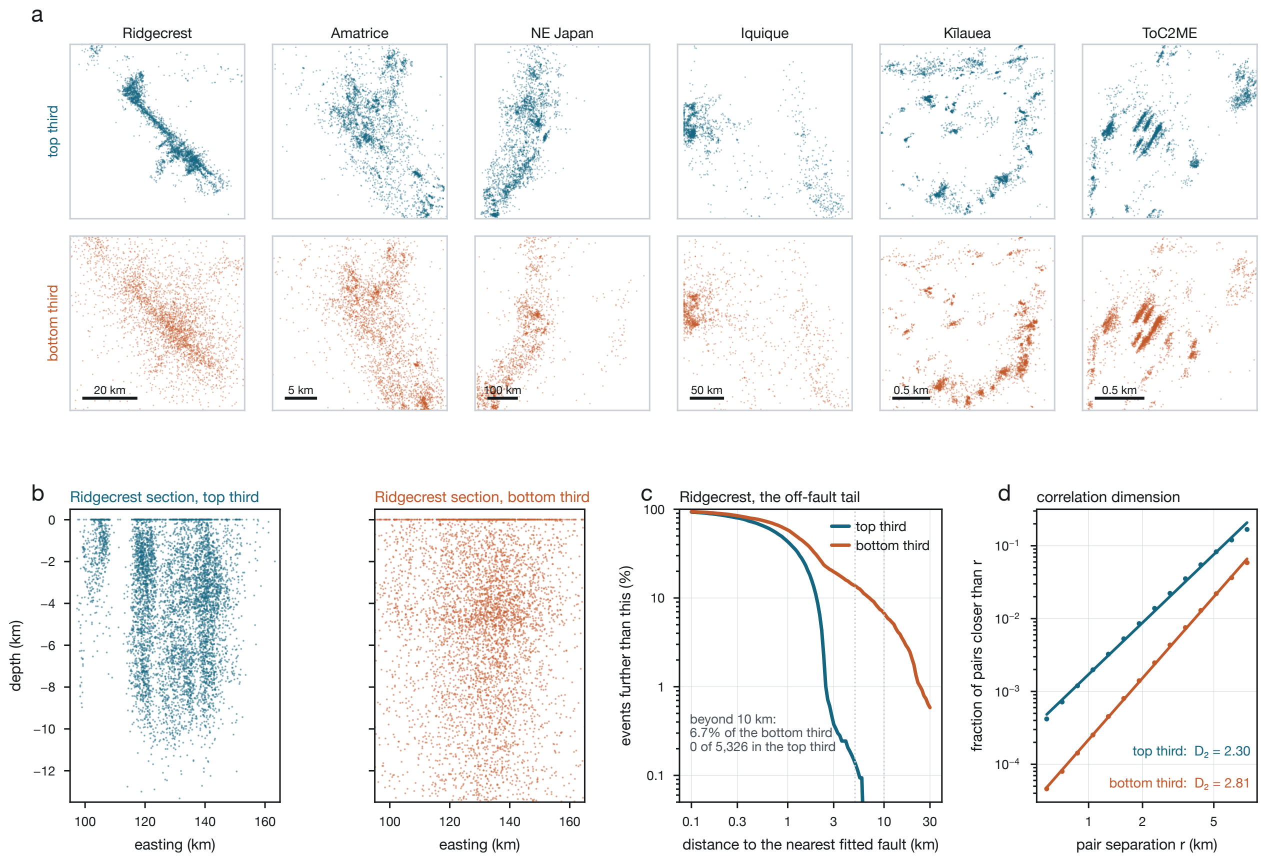

Fig. 3 | Where the lowest-ranked events sit. Every event carries a confirmability score fitted to seven quantities the catalogue already records, and the top and bottom thirds by that score are compared in **a** to **c**; **d** uses the top and bottom quartiles, which is what the correlation integral requires. How the two thirds are equalised differs by panel and is stated in each: the maps and section are drawn to a common magnitude and depth histogram, the fault-distance statistic to a common magnitude histogram, and D_2 at equal sample size (Methods). **a**, Map view of the top third (blue) and bottom third (orange) for the six sequence catalogues, each drawn to its own extent with a scale bar. Kīlauea and ToC2ME span too short a range of separations for D_2 to be measured and are shown for completeness; their fitted fault networks are reported in Table S10. **b**, The Ridgecrest thirds in east–west cross-section. **c**, The off-fault tail at Ridgecrest: the fraction of each third that lies further than a given distance from every segment of a fault network fitted to a random, score-blind half of the catalogue. The medians of the two thirds differ by only 0.4 km, although the tails do not, and beyond 8 km no event of the 5,326 in the top third is found at all. **d**, The correlation dimension D_2 at Ridgecrest, on the top and bottom quartiles by score, the exponent with which the number of event pairs closer together than r grows with r: near 1 for events on a line, 2 on a plane and 3 filling a volume. The bottom third is closer to filling a volume, as it is in all four catalogues where D_2 can be measured (Fig. S4). Restricting the comparison to events the human-reviewed catalogue independently contains leaves most of the D_2 contrast standing but removes the off-fault tail (Fig. S5).

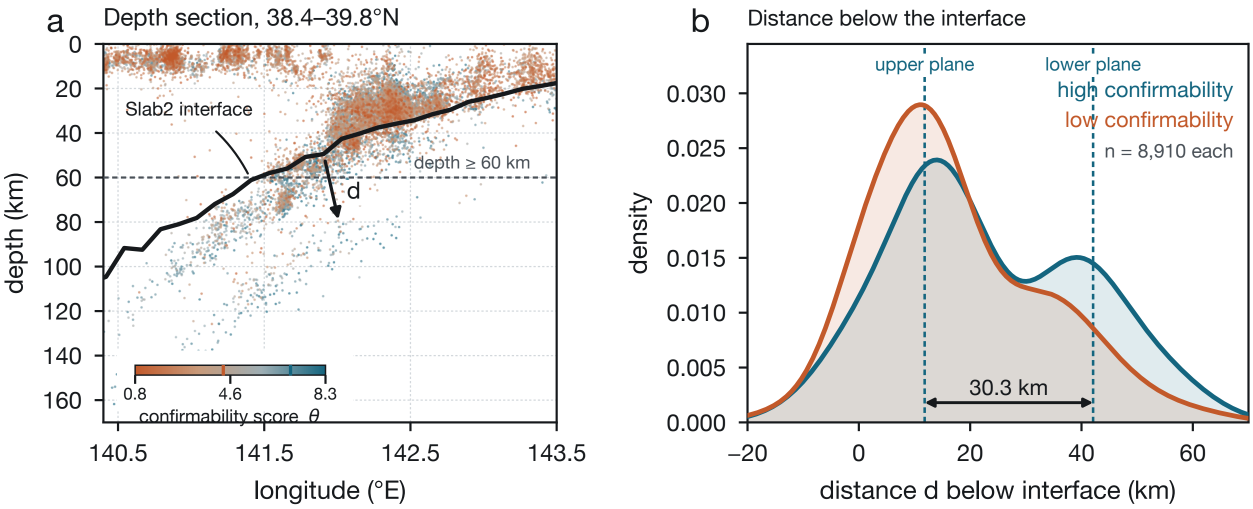

Fig. 4 | The lowest-ranked events blur a real structure. **a**, Depth section of the NE Japan forearc catalogue between 38.4 and 39.8°N, coloured by confirmability score, with the Slab2 plate-interface model in black. Intraslab earthquakes below the interface form two sub-parallel planes about 30 km apart, the double seismic zone; the analysis uses events deeper than 60 km and measures each one's perpendicular distance d below the interface. **b**, The distribution of d for the top (blue) and bottom (orange) quartiles by confirmability score, drawn to equal size. Both show the upper plane; the lower plane is distinct in the top quartile and only a shoulder in the bottom quartile. The separation of the two planes relative to their width, from a two-component Gaussian mixture, is 3.25 in the top quartile against 2.86 in the bottom, a difference of +0.39 (95% CI +0.34 to +0.45), and the fitted spacing of 30.3 km matches the published value. The quartiles are equalised in size and in depth here but not in magnitude; drawing the top quartile to the bottom quartile's magnitude histogram as well leaves +0.339 (+0.155 to +0.538), with the two medians still 1.72 against 1.11 (Table S7). Injecting depth error into the top quartile shows that reproducing the loss of separation would require about three times the depth uncertainty the bottom quartile is measured to carry (Fig. S6).

Supplementary Information

How much of a machine-learning earthquake catalogue can an expert verify?
Meng, Huang, Ma & Ma

Table S1 | The eight audited catalogues

sequence	setting	candidate catalogue	dataset DOI	scored events	frame	frame covers	panel
Ridgecrest	2019 M7.1 strike-slip sequence, California	this study (PhaseNet + PyOcto + ADLoc)	—	137,703	134,056	97.4%	200
Iquique	2014 M8.1 subduction sequence, northern Chile	this study (PhaseNet + PyOcto + ADLoc)	—	6,968	4,832	69.3%	200
Amatrice	2016–17 central Italy normal-faulting sequence	Tan et al. 2021, CAT5	10.5281/zenodo.4736089	113,396	112,668	99.4%	200
Japan forearc	NE Japan subduction forearc	Suzuki et al. 2025	10.5281/zenodo.13854225	627,435	627,435	100.0%	200
ToC2ME	2016 hydraulic-fracturing experiment, Alberta	Igonin et al. 2020, `Catalog_Igonin2020_Beamforming.csv`	github.com/nadineigonin/ToC2ME (paper: 10.1029/2020JB020311)	18,040	18,040	100.0%	200
Kīlauea	2018 caldera-collapse sequence, Hawai'i	this study (PhaseNet + PyOcto + ADLoc)	—	44,188	38,203	86.5%	200
Ridgecrest, Shelly	the same 2019 sequence, 4–16 July	Shelly 2020, template matching + relative relocation	USGS ScienceBase	34,091	34,091	100.0%	200, one reviewer
Ridgecrest, QTM	the same 2019 sequence	Ross et al. 2019, template matching + GrowClust	SCEDC	111,918	111,918	100.0%	200, one reviewer

Three of the six sequence catalogues were built for this study (Ridgecrest, Iquique and Kīlauea); the two further Ridgecrest catalogues were reviewed by one of the four reviewers and enter only the three-catalogue comparison. The other three, Amatrice, the NE Japan forearc and the Igonin et al. beamforming catalogue at ToC2ME, are published community products audited as distributed, so the picking, association and location choices are the original authors'. Auditing the distributed product instead of a reproduction of it is deliberate: the product is what the community uses.

Every sequence panel is 200 events judged by all four reviewers; the two further Ridgecrest catalogues are 200 events each judged by one of them. Ridgecrest was originally designed at 500 events for a single-reviewer pass; that pass used a different review interface and is not used, so the 200-event blind panel is the one every Ridgecrest number comes from.

Table S2 | Stratification and design weights

sequence	strata	population covered	design-weight range
Ridgecrest	24	134,056	6.8 – 1500.7
Iquique	18	4,832	1.0 – 35.9
Amatrice	21	112,668	1.0 – 839.7
Japan forearc	18	627,435	106.8 – 4258.9
ToC2ME	32	18,040	1.0 – 165.7
Kīlauea	18	38,203	137.3 – 231.3

Sampling is deliberately disproportionate: a floor of five events per non-empty stratum guarantees that rare cells carrying large population weight are represented, and this is what allows a 200-event panel to say something about a catalogue that may be thousands of times larger. Population estimates are correspondingly design-weighted, and confidence intervals come from a stratified bootstrap resampling within strata.

How much does any one cell carry? The design weights are deliberately uneven, so we refitted the estimate with each stratum dropped in turn, and again with each adjudicated event dropped in turn.

sequence	strata	heaviest stratum, events per adjudication	worst leave-one-stratum-out	worst leave-one-event-out
ridgecrest	24	1,501	+3.6 pts	1.3 pts
iquique	18	36	+0.4 pts	0.8 pts
amatrice	21	840	-3.0 pts	1.0 pts
japan_forearc	18	4,259	+4.1 pts	0.8 pts
toc2me	32	166	+4.0 pts	1.0 pts
hawaii_kilauea	18	231	+1.2 pts	0.6 pts

No stratum moves any estimate by more than 4.1 points and no single adjudicated event by more than 1.3, against confidence intervals 4 to 16 points wide (Table S9). The estimates are not carried by one cell.

Table S3 | Model variants

Scored against the blind panel consensus (plurality of four verdicts, ties counted as uncertain) under stratified five-fold cross-validation.

variant	features	n	AUC	95% CI	Brier
all association features	7	151	0.946	[0.905, 0.978]	0.075
three features	3	151	0.926	[0.861, 0.967]	0.078
+ reference-catalogue match	8	151	0.940	[0.896, 0.975]	0.078

Three features, namely phase count, station count and the move-out residual, reach AUC 0.926, against 0.946 for the full association model. Most of the discriminating information is concentrated in a few physical quantities and not spread across the set, though the remaining four features are not quite redundant.

Adding agreement with an independent high-resolution catalogue does not help. However, it moves AUC to 0.940, below the model without it. Whatever information the match carries about confirmability is already present in the waveform evidence, and the extra parameter costs more than it returns. That is the quantitative reason we do not treat catalogue agreement as ground truth.

Expected calibration error over five equal-width bins, i.e. the average gap between the confidence a rule implies for a detection and the fraction of such detections the panel confirms. Both weightings are given: the panel column describes the 200 adjudications, the catalogue column applies the design weights and is the one the main text quotes, since it describes the catalogue (Methods).

calibration	gap, panel-weighted	gap, design-weighted
raw model	0.018	0.040
after Platt scaling	0.025	—
signal-to-noise threshold	0.185	0.185
pick-count threshold	0.107	0.145
reference-catalogue match	0.417	0.499

Table S4 | Transfer across catalogues and reviewers

The Ridgecrest-fitted score applied **unchanged** to the two other catalogues carrying the same association features, scored against each reviewer's own blind verdicts. AUC is reported only where a reviewer returned at least ten false verdicts; below that the negative class is too small for the statistic to mean anything.

catalogue	reviewer	events	false verdicts	AUC
ridgecrest	Yang Ma	135	31	0.944
ridgecrest	Hui Huang	164	37	0.931
ridgecrest	Jinzhi Ma	180	3	not estimable
ridgecrest	Lingsen Meng	162	39	0.914
iquique	Hui Huang	196	6	not estimable
iquique	Yang Ma	146	10	0.674
iquique	Jinzhi Ma	195	1	not estimable
iquique	Lingsen Meng	172	4	not estimable
japan_forearc	Hui Huang	174	34	0.766
japan_forearc	Lingsen Meng	174	26	0.727
japan_forearc	Jinzhi Ma	181	2	not estimable
japan_forearc	Yang Ma	126	30	0.789

Median AUC over the 7 estimable units is 0.789 (range 0.674–0.944). That pooled figure mixes the region the model was fitted in with the regions it had never seen, and the two differ: the median is 0.931 across the 3 Ridgecrest units and 0.747 across the 4 external ones. 5 of the 12 units returned too few false verdicts to estimate an AUC at all, and are listed above without one.

What does not transfer. Score distributions shift substantially between catalogues, so a threshold chosen at Ridgecrest neither retains a comparable fraction nor delivers comparable precision elsewhere. Transport the ranking; refit the level locally.

Table S5 | Reviewer leniency model

label	reviewer	leniency *b*	raw confirmation rate	rate at the common threshold
R1	Jinzhi Ma	-3.053	90.9%	76.3%
R2	Lingsen Meng	+0.468	70.9%	76.3%
R3	Hui Huang	+0.574	72.8%	76.3%
R4	Yang Ma	+2.011	50.3%	76.3%

R1–R4 are the labels used in Fig. 2a,b and Fig. S1b, ordered from most to least lenient; the labels keep the figures readable and are mapped here. All four adjudicators are authors of this paper, which is a limitation of the study: the panel is not independent of the investigators, and blinding is what stands in for that independence.

Fitted on 4,800 verdicts over 1,200 events; converged in 14 profile iterations with cut points at [-1.0, 1.0] and $\Sigma b = 0$. Reproduces 89.5% of individual verdicts.

Because all four reviewers judged the identical 1,200 events, removing leniency makes the four corrected rates equal by construction; the informative quantity is that a 41-point raw spread is fully accounted for by four reviewer-specific thresholds.

Predictive check. Each verdict was held out in turn and predicted from the other three verdicts on the same event, with the reviewer's leniency held at its full-sample value. For the three stricter reviewers the model beats an "always confirm" baseline by 7.4 to 14.5 points. For the most lenient reviewer it does not (90.0% against 90.9%): a reviewer who confirms 91% of what they see carries little information with which to predict them, and the model gains nothing on that reviewer even though it correctly recovers their leniency.

Table S6 | Correlation dimension: scaling window and ladder

D_2 is a scaling exponent and is only defined where $C(r)$ actually scales. The fitting window is therefore measured per region as the range over which $C(r)$ neither saturates nor empties, and D_2 is declined where that range is shorter than 1 decade.

region	fitting window	decades	D_2 high	D_2 low	raw	geometry	+ magnitude
Ridgecrest	0.58–7.67 km	1.12	2.30	2.81	+0.507	+0.284	+0.285
Iquique	1.05–19.57 km	1.27	2.17	2.27	+0.100	+0.127	+0.127
Amatrice	0.18–4.80 km	1.42	1.65	2.28	+0.624	+0.602	+0.692
Japan forearc	1.49–63.10 km	1.63	1.56	1.83	+0.264	+0.236	+0.279
ToC2ME	—	0.46	*not reported*				
Kīlauea	—	0.97	*not reported*				

Values are D_2(low confirmability) – D_2(high confirmability); positive means high-confirmability events are more surface-like. Groups are compared at equal sample size.

Within magnitude strata, where both subsets share the same location constraint by construction:

region	magnitude stratum	n per group	D_2 difference
Ridgecrest	0.0-0.5	4,000	+0.308
Ridgecrest	0.5-1.0	4,000	+0.508
Ridgecrest	1.0-1.5	4,000	+0.540
Ridgecrest	1.5-2.0	2,369	+0.594
Amatrice	0.0-0.5	2,281	+0.751
Amatrice	0.5-1.0	4,000	+0.674
Amatrice	1.0-1.5	4,000	+0.493
Amatrice	1.5-2.0	1,953	+0.430
Japan forearc	0.5-1.0	1,367	+0.284
Japan forearc	1.0-1.5	2,965	+0.392
Japan forearc	1.5-2.0	2,555	+0.587
Japan forearc	2.0-5.0	2,275	+0.437

Which covariates are controlled. Network geometry is a *confounder*, since a denser sub-network both raises the score and tightens locations, and is removed. Signal-to-noise and the move-out residual are *mediators*, the channel through which a spurious detection reveals itself, so removing them removes the effect under test (regressing out four signal-to-noise features drives the Ridgecrest difference to +0.08; Note S4). Location uncertainty is the ambiguous case, partly a mediator and partly a competing explanation, and we do not treat controlling for it as decisive either way (Note S4).

At Amatrice the only network-geometry quantity recorded is the number of stations that returned a trace, with no azimuthal coverage, so the control there is a station-count control and is weaker than the control applied elsewhere.

Table S7 | Double seismic zone

Depth $\geq$ 60 km; n = 35,640. High confirmability = top 25% (score $\geq$ 6.9370); low confirmability = bottom 25% (score $\leq$ 4.2780).

stratum	n per group	high: two planes	low: two planes	separation (high)
pooled $\geq$ 60 km	8,910	30/30	0/30	30.3 $\pm$ 0.0 km
60–80 km	4,474	0/30	0/30	8.5 km
80–100 km	2,138	30/30	30/30	24.1 km
100–150 km	1,046	30/30	0/30	25.0 km

The depth bands hold 7,658 events per group against 8,910 pooled: the remaining 1,252 lie below 150 km depth and enter the pooled row only, there being too few of them per group to resolve a density in a band of their own.

Magnitude-matched contrast. Low-score events are most of the small-magnitude population, so the raw quartile contrast confounds confirmability with event size. Drawing the high-score group to the low-score group's own magnitude histogram gives:

	separation ratio	two-plane draws	n per group	median M
high, unmatched	3.254	30/30	8,910	2.21
high, matched	3.219	30/30	1,856	1.72
low	2.880	2/30	1,856	1.11

Matching narrows the separation-ratio difference from +0.393 (95% CI +0.337 to +0.450) to +0.339 (+0.155 to +0.538), high above low in 39/40 draws. The match is close but not exact: the high-score group has too few of the smallest events to fill the low-score histogram completely, so its median magnitude falls from 2.21 to 1.72 against 1.11. Magnitude therefore accounts for part of the contrast and not for the whole of it.

Contamination sweep. Fraction of the high-score sample replaced by low-score events:

low-score fraction	0%	20%	40%	60%	80%	100%
two-plane draws	30/30	30/30	30/30	30/30	8/30	0/30

Noise-injection control. Gaussian depth error added to the high-confirmability population:

added σ (km)	0	1	2	3	3.5	4	4.5	5	5.5	6	7	8	10	12
two-plane draws (%)	100	100	100	100	100	100	100	68	8	0	0	0	0	0

Critical σ = 5.5 km. The low-confirmability group's median formal depth uncertainty is 1.79 km against 0.70 km for the high-confirmability group, an excess of ~1.65 km, about a third of what would be needed to erase a plane. Location precision is quantitatively insufficient as an explanation.

Table S8 | The scoring model

Standardised ridge coefficients for each catalogue's score, all predicting the same target: the latent event quality theta from the blind leniency model. A positive weight pushes the score toward *real*.

ridgecrest, iquique, japan_forearc

feature	ridgecrest	iquique	japan_forearc
`az_gap`	-0.500	-0.189	-0.351
`dist_nearest_sta_km`	-0.528	+0.096	+0.435
`mag`	-0.338	+0.000	-0.227
`moveout_rms`	-1.069	+0.073	-0.041
`n_pha_total`	+1.013	+0.557	+1.109
`n_sta`	+0.788	+0.582	+1.161
`sec_az_gap`	-0.430	-0.220	+0.395

amatrice

feature	amatrice
`max_snr`	+0.224
`med_snr`	+0.257
`moveout_rms_comp`	-0.323
`n_snr_ge2p5`	+2.876
`n_snr_ge4`	-0.719
`n_sta_read`	+0.830

toc2me, hawaii_kilauea

feature	toc2me	hawaii_kilauea
`max_snr_adapt`	+0.749	+0.317
`max_snr_common`	+0.383	+0.245
`med_snr_common`	+0.311	+0.425
`moveout_rms_adapt`	-0.385	-0.009
`moveout_rms_common`	-0.141	-0.161
`n_snr_ge2p5_common`	+0.214	+0.607
`n_snr_ge4_common`	-0.139	+0.506
`n_sta_read`	+0.000	-0.010

Out-of-fold rank correlation against theta, by catalogue: ridgecrest +0.72, iquique +0.44, japan_forearc +0.54, amatrice +0.75, toc2me +0.59, hawaii_kilauea +0.68.

Table S9 | Design-weighted population estimates by sequence

The panels are disproportionately stratified samples, so a raw panel rate describes the panel and not the catalogue. Each panel event is therefore weighted by the number of catalogue events in its stratum. The estimator is the ratio of the design-weighted real share to the design-weighted decided share; the bracket is what that becomes when every event the panel declined is assigned first to false and then to real.

sequence	population estimate	95% CI	bracket
Kīlauea	97.6%	95.5–99.4%	93.3–97.7%
Iquique	97.3%	94.4–99.6%	85.7–97.7%
Amatrice	95.5%	91.7–98.5%	70.1–96.7%
Ridgecrest	85.3%	78.1–91.9%	58.7–89.8%
NE Japan forearc	84.1%	78.6–89.1%	70.7–86.6%
ToC2ME	60.1%	52.1–68.1%	42.4–71.8%

The estimates run 60.1–97.6% with a median of 90.4%. The lowest is ToC2ME, a hydraulic-fracturing catalogue of very small events recorded on a small array; the highest are the two subduction sequences and the caldera collapse. Ridgecrest carries the widest bracket, because it has by far the largest share of detections the panel declined to call either way.

Table S10 | Fault-segment fitting: parameters and comparison

E2F carries two length scales and neither has a default that travels between sequences. The Hough discretisation defaults to 1/64 of the extent of the seismicity, and the control scale multiplies a magnitude-derived radius whose published optima span a factor of thirty. Both are therefore scanned per catalogue and held identical across the groups compared within it. The reported quantity is the fraction of a group's events placed in a segment of at least fifty events; groups are equal in size and matched bin by bin in magnitude. Each third is drawn ten times and the null twenty times; ranges are over draws, and the last three columns are the fraction of draw pairings in which the stated comparison holds.

catalogue	events per group	dx (km)	C	top third	bottom third	twenty random draws	top over bottom	top over random	bottom under random
Ridgecrest	8,627	3.604	305.1	0.924 (0.910–0.940)	0.426 (0.403–0.444)	0.664–0.734	1.00	1.00	1.00
Iquique	2,322	8.83	499.4	0.547 (0.547–0.547)	0.193 (0.193–0.193)	0.321–0.410	1.00	1.00	1.00
NE Japan forearc	3,669	16.94	714.6	0.484 (0.440–0.535)	0.206 (0.171–0.225)	0.252–0.448	1.00	0.99	1.00
Amatrice	16,811	2.752	263	0.946 (0.941–0.955)	0.859 (0.847–0.864)	0.896–0.919	1.00	1.00	1.00
Kīlauea	7,662	0.5643	2.3	0.539 (0.497–0.611)	0.414 (0.398–0.419)	0.412–0.600	1.00	0.91	0.96
ToC2ME	4,278	0.0853	38.9	0.792 (0.740–0.834)	0.772 (0.752–0.787)	0.750–0.808	0.64	0.66	0.46

The score orders the two thirds in five of the six catalogues without an exception among the hundred pairings, ToC2ME alone falling to 0.64. Separation from a typical slice of the same catalogue is complete at Ridgecrest, Iquique and Amatrice and almost complete in NE Japan; at Kīlauea the ordering holds in every pairing although both thirds sit within the spread of the random draws. Kīlauea and ToC2ME are also the two sequences too spatially compact to carry a correlation-dimension scaling range.

Table S11 | Fault-segment fitting: robustness

The fifty-event floor that defines a resolvable segment is ours and not E2F's, so the contrast is reported across a twentyfold range of it. Location precision is not removed from the score; instead the high-scoring group is blurred with isotropic Gaussian position error and the blur needed to reproduce the contrast is compared with the extra location scatter the low-scoring group actually carries. Only the NE Japan catalogue publishes a location uncertainty, so it is the only sequence where that comparison closes.

catalogue	$n \geq 10$	$n \geq 30$	$n \geq 50$	$n \geq 100$	$n \geq 200$	blur needed	observed extra scatter
Ridgecrest	+0.490	+0.500	+0.496	+0.497	+0.500	8 km	not published
Iquique	+0.390	+0.353	+0.353	+0.364	+0.280	12 km	not published
NE Japan forearc	+0.350	+0.267	+0.246	+0.232	+0.189	>12 km	2.46 km
Amatrice	+0.086	+0.088	+0.087	+0.087	+0.073	—	not published
Kīlauea	+0.159	+0.185	+0.201	+0.154	+0.161	—	not published
ToC2ME	+0.006	+0.052	+0.063	-0.003	-0.046	—	not published

Each cell is the top third minus the bottom third, on the first draw of each. The four significant contrasts are flat across the whole range, so the floor is not producing them. In NE Japan reproducing the contrast requires more than 12 km of blur against the 2.46 km of extra scatter observed, which indicates that location precision is not a sufficient explanation.

Note S1 | Why agreement with a reference catalogue is not ground truth

Two substitutes are in common use: a signal-to-noise threshold on the waveform, and agreement with an independent, higher-resolution catalogue. Neither can serve as truth, and they fail for different reasons, so no single correction repairs both.

The signal-to-noise threshold measures the threshold. Applying a maximum-SNR rule to the same 200 panel events under the same design weights, the implied real fraction of the Ridgecrest catalogue is 76.0% at a threshold of 3, against 85.3% from the panel. However, the number moves with the threshold and not with the catalogue:

max SNR threshold	implied real fraction	share of the panel kept
2.0	87.8%	82%
2.5	80.2%	75%
3.0	76.0%	70%
4.0	60.1%	58%
5.0	51.7%	50%

A rule whose answer slides by 36 points over the range of thresholds a practitioner might reasonably pick is not measuring the quantity it is being asked for. It is also the substitute that a real but small event fails by construction, which is the same population the panel finds hardest.

The other substitute, matching to a reference catalogue, fails differently.

It is biased low. Using matching as the criterion estimates the Ridgecrest real fraction at 35.2%, against 85.3% from the blind panel. A real event that the reference catalogue missed is counted as false, and the reference catalogues miss a great deal.

It disagrees with itself. The reference catalogues do not agree with each other. Against the same candidate catalogue, in the same space-time window and with a deliberately generous 3 s / 15 km matching gate, three times the radius used for the reference control in the main text:

reference	events in window	candidate detections matched
QTM template-matched	111,918	35.2%
Shelly relocated	34,091	42.1%
SCSN analyst	27,981	16.3%

The three disagree by a factor of more than two on how much of the same catalogue they corroborate. A criterion that changes this much with the choice of reference is not a measurement of reality.

It is redundant. Adding “matches the reference catalogue” as a model feature moves AUC to 0.940, below the 0.946 of the model without it (Table S3). Whatever information the match carries about confirmability is already present in the waveform.

Note S2 | The temporal-permutation floor, and what it does not say

To bound how much of an associator’s yield could arise from timing coincidence alone, we circularly shifted each station’s picks independently within the UTC day. This destroys genuine cross-station move-out while preserving each station’s pick count, phase mix and inter-pick-time statistics exactly, then re-ran association with the identical configuration.

day	real events	median null events	floor
2019-07-06	5,550	9,378	169%
2019-07-20	5,289	7,870	149%
2019-07-28	4,867	7,120	146%

This is not a false-discovery rate and must not be quoted as one, and it is also not a bound on the real catalogue. Real picks are clustered in time, because aftershocks arrive in bursts, and a circular shift within the day spreads that clustering uniformly, which raises the coincidence rate on its own; that the shuffled input yields more events than the real one is therefore a property of the shuffle and not evidence about the catalogue. What the table does show is narrower: fed picks with no genuine move-out at these rates, the associator returns thousands of events per day, so its yield is not by itself evidence that anything seismic occurred. That is the motivation for waveform verification, and it is all this note claims.

Note S3 | Why we do not interpret the depth dependence of the plane separation

Our measured plane separation increases with depth (8.5 km at 60–80 km, 24.1 km at 80–100 km, 25.0 km at 100–150 km), the opposite of the convergence reported in the literature. The cause is a depth-dependent offset between Slab2 and this catalogue's depths, and restricting to Tohoku (37–41.5° N) does not remove it. Slab2 therefore enters only as a common reference surface, measured identically for both score groups at the same depth, so the high-versus-low contrast is unaffected by the offset. We make no claim about depth dependence.

Note S4 | What the geometry control does not settle

The score is trained on what an expert will endorse, and the features it is built from (phase count, move-out consistency, network geometry) are the same quantities that determine how precisely an event can be located. Filtering on it and finding sharper structure is therefore consistent with two readings: that the discarded events are spurious, or that they are merely the badly located ones. Both would sharpen a fault plane. This note gives the size of the problem.

Standardised mean differences between the top and bottom score quartiles at Ridgecrest, before and after removing network geometry by polynomial residualisation:

feature	SMD raw	SMD after geometry	role
`n_sta`	+3.223	+0.023	confounder (controlled)
`az_gap`	-2.781	-0.053	confounder (controlled)
`sec_az_gap`	-1.828	-0.021	confounder (controlled)
`dist_nearest_sta_km`	-1.077	-0.031	confounder (controlled)
`n_pha_total`	+3.075	+0.254	mediator (deliberately not controlled)
`moveout_rms`	-2.556	-4.046	mediator (deliberately not controlled)

The control does what it targets: the four geometry covariates come to within 0.02–0.05 standardised units. However, the two mediators are another matter. Phase count still differs by 0.25, and the move-out residual by 4.05, so the groups are all but disjoint on the single quantity most directly tied to location quality. Controlling for it would remove the evidence the score is built from, and the difference under test would go to zero by construction.

Three things bound the reading, none of them decisive.

1. **The score is not a size filter.** Magnitude alone separates the classes at AUC 0.556, and removing magnitude from the full model moves it from 0.946 to 0.941.
2. **The double seismic zone statistic is not one that location error shifts.** Where events sit relative to the slab interface is depth-matched and equal-sized between the groups, and imprecise locations broaden that distribution instead of displacing it. The noise-injection test puts the broadening required to erase the second plane at 5.5 km against the 1.65 km the low-confirmability group carries.
3. **The uncertainties that argument rests on are the catalogue's own.** They have not been externally calibrated, and that limits the bound in point 2.

Since this note was first written, one independent handle has become available at Ridgecrest, and it is reported in the main text. Restricting to the 20,588 detections the human-reviewed regional catalogue independently contains, none of which can be false, the confirmability score still orders D_2 by +0.37 against +0.50 in the full catalogue (Fig. S4c), so three quarters of the D_2 contrast is reproduced among events that are real on outside authority; D_2 is accordingly read as a statement about catalogue quality. The off-fault tail behaves differently: the fraction of the bottom third beyond 10 km from any fitted fault falls from 6.7% to 0.4% in the same subset, and the contrast does not return when the match radius is widened to 15 km (Fig. S5c). The tail is therefore concentrated in machine-only detections. Whether those are false could only be tested against the panel's own verdicts, and at 200 events that test is a null with a standard error of 0.11 in $\log_{10}$ distance against a full-catalogue effect of about 0.15 (Fig. S5d), which is a statement about power and not about absence.

What the downstream results support is that events an expert panel will endorse carry more coherent catalogue structure than events it will not, and that a score can identify them in advance. What they do not establish is that the unendorsed events are not earthquakes. Distinguishing those would take an independent handle on truth this design does not have, namely dense-array or template-matched confirmation of the specific detections the panel declined. That is the experiment this work argues should follow it, not one it contains.

Note S5 | How the waveform features are measured

Three of the six catalogues, Amatrice, ToC2ME and Kīlauea, distribute no association-stage record, so the features their confirmability score is built from were measured here from the waveforms alone plus the candidate hypocentre, blind to the verdicts (Methods). This note gives those measurements in full.

Signal-to-noise ratios. For each event and station we compute SNR as the ratio of root-mean-square amplitude in a signal window following the predicted P arrival to that in a preceding noise window. Window lengths adapt to the catalogue's origin-time precision t_p: for finely resolved catalogues ($t_p \leq 0.05$ s) the signal window is $[0,\ 1.5]$ s after the pick with a 5 s noise window ending at the pick; for coarser catalogues the signal window is widened to $[-0.6\,t_p,\ \max(1.5,\ 0.6\,t_p)]$ with a guard band of $2t_p$ separating signal from noise. This adaptation is not cosmetic. At ToC2ME the catalogue quantises origin times to 1 s; with fixed windows the "noise" window swallowed the signal, which inverted the discriminant and produced AUC ≈ 0 until the quantisation was accounted for.

SNR is computed in two passbands. The common band is fixed across all events in a region and permits like-for-like comparison. The adaptive band follows the physics:

$$f_{\mathrm{hi}} = \min\left(3f_c,\ \frac{1}{\pi t^*},\ 0.4\,f_{\mathrm{Nyq}}\right), \qquad f_{\mathrm{lo}} = \max(1\ \mathrm{Hz},\ 1.5\,f_{\mathrm{sensor}})\,.$$

The three terms bounding f_{hi} are the source, the path and the recording. The first is the Madariaga[24] corner frequency for an event of seismic moment M_0,

$$f_c = K\beta\left(\frac{\Delta\sigma}{M_0}\right)^{1/3}, \qquad K = 0.21,\ \beta = 3500\ \mathrm{m\,s^{-1}},\ \Delta\sigma = 3\ \mathrm{MPa};$$

the second is the Anderson–Hough[25] attenuation cutoff, with $t^* = R/(vQ)$ for hypocentral distance R, path velocity v and quality factor Q; the third is the anti-alias limit. The lower corner is set by the noise floor and the instrument, not by the source, and that choice matters. Tying it to the source instead, at $f_c/4$ say, fails because the displacement spectrum is flat below f_c: excluding that band discards the strongest part of the signal, and in five of seven settings it leaves a band narrower than an octave. Bands narrower than one octave are returned as missing and not forced. Sensor corners are tabulated per network with provenance; the

S-net corner of 15 Hz is from Uchida et al.[26] and is verified. The ToC2ME 5B corner of 10 Hz is taken from the array's own documentation and could not be verified against an instrument response. It sets the adaptive band's lower bound at ToC2ME, and two adaptive-band features enter that sequence's score, one of them with the largest weight in the model. We therefore bounded what it can carry: refitting the ToC2ME score on the corner-independent fixed-band features alone lowers the out-of-fold rank correlation with θ from +0.593 to +0.463, and the two rankings agree at ρ = +0.801. The corner contributes, but no value of it can overturn the ToC2ME ranking.

Move-out residual. For each event we compute the root-mean-square misfit between observed picks and the arrival times predicted by a 1-D velocity model from the candidate hypocentre. Regional velocities are taken from the source study where one exists; for Hawai'i we measured the effective travel-time relation directly from the data ($t = 0.441 + R/4.67$ s), because the nominal $V_P = 5.0$ km s^{-1} was badly wrong (measured 2.86 km s^{-1}) and mis-specified windows for the 13.8% of events at large distance. Only stations whose SNR exceeds a gate enter the residual. The gate was tuned at Ridgecrest (SNR ≥ 2.5); at ToC2ME that value left the residual computable for only 11 of 200 panel events, so it was relaxed to 1.2, which recovers move-out as the third-strongest feature with the physically correct negative sign. The gate is reported per region.

Station support. The number of channels exceeding fixed SNR thresholds (2.5 and 4.0), and the number of stations contributing to the move-out residual.

Note S6 | The two fits of the confirmability score, and how calibration is measured

The confirmability score is fitted twice: as a ranking on all six catalogues, and as a confirmation probability at Ridgecrest (Methods). This note gives both estimators, the rescaling we tried and did not use, and the definition of the calibration error quoted in the main text.

As a ranking. The score is a ridge regression predicting the latent event quality θ of the leniency model. For standardised features X and penalty λ,

$$\hat{\mathbf{w}} = \arg\min_{\mathbf{w}} \|\boldsymbol{\theta} - X\mathbf{w}\|_2^2 + \lambda\|\mathbf{w}\|_2^2,$$

with λ chosen by cross-validation over twenty logarithmically spaced values in $[10^{-2}, 10^{3}]$, and performance reported as the rank correlation between the out-of-fold prediction and θ under five-fold cross-validation (the target is continuous, so the folds are not stratified; stratified folds are used for the binary model). Regressing on θ instead of on a thresholded label is what lets the same method serve all six sequences. Three of them will not support a binary classifier: the Kīlauea panel resolves 185 confirmed against only 5 rejected, ToC2ME's quantised origin times leave the move-out feature missing for most events at the Ridgecrest gate, and Amatrice's published catalogue carries no association-stage record at all, so its features had to be measured from the waveforms for this study. For those three the continuous score is the only score we report.

As a probability, at Ridgecrest. The model is ℓ_2-regularised logistic regression on the binary panel label, confirmed against rejected, with the events the panel left unresolved excluded. Writing $\sigma(u) = (1 + e^{-u})^{-1}$ and $p_i = \sigma(\beta_0 + \boldsymbol{\beta}^\top \mathbf{x}_i)$,

$$(\hat{\beta}_0, \hat{\boldsymbol{\beta}}) = \arg\min \; -\sum_i \Big[y_i \log p_i + (1 - y_i)\log(1 - p_i) \Big] \; + \; \frac{1}{2C}\|\boldsymbol{\beta}\|_2^2,$$

at fixed $C = 1$. We did not tune C: with seven features and 151 resolved events the fit is not penalty-sensitive, and leaving it fixed removes one investigator degree of freedom. Features are standardised using the training fold's own mean and standard deviation, so no information crosses the fold boundary.

Rescaling was tried and is not used. The standard remedy for a miscalibrated classifier is Platt scaling[23], a two-parameter monotone rescaling $p^{\mathrm{cal}} = \sigma(A\log[p/(1-p)] + B)$. Being monotone it cannot change the ranking or the AUC, only what the numbers mean. Applied here it moves the calibration error from 0.018 to 0.025, slightly worse because the raw score is already close to calibrated, so we report the score as it comes. The two parameters were fitted on the out-of-fold scores and applied to those same scores, which is mildly optimistic for the rescaled curve and therefore only strengthens the conclusion that the rescaling is not worth applying.

Calibration error. Reliability is summarised over B probability bins as the expected calibration error, with each bin weighted by the share of the population it carries,

$$\mathrm{ECE} = \sum_{b=1}^{B} \frac{W_b}{W} \left|\bar{p}_b - \bar{y}_b\right|, \qquad \mathrm{MCE} = \max_b \left|\bar{p}_b - \bar{y}_b\right|,$$

where $\bar{p}_b$ is the mean predicted probability in bin b, $\bar{y}_b$ the observed fraction of real events in it, and W_b the total weight it holds. Setting every weight to one gives the panel figure; using the design weights gives the catalogue figure.

Both the binning and the weighting matter, so we report all four combinations. With $B = 5$ equal-width bins the ECE is 0.018 on the panel and 0.040 design-weighted, and the corresponding maxima are 0.127 and 0.196. With equal-count bins, which cannot leave a bin nearly empty and then weight its gap as though it were full, the ECE is 0.016 either way and the maxima are 0.028 and 0.034. The equal-width maxima are driven by the sparsely populated extreme bins; the equal-count figures are the more stable summary, and the equal-width design-weighted ECE of 0.040 is the most conservative. We quote 0.040 in the Results for that reason.

Note S7 | The panel design, and what a partially filled stratified panel does

The panel was designed around a two-reviewer agreement gate declared before the verdicts were read. On the first two reviewers the gate failed, with design-weighted three-class kappa of 0.254 against a declared threshold of 0.60. The disagreement it detected was a difference in threshold between reviewers and not noise, which further reviews of the same kind would not have resolved, so we changed the design to four reviewers each judging all 200 events in every sequence, fully crossed. A crossed design identifies that difference and removes it, which a partially overlapping one cannot. Kappa on the four-way panel is not the quantity of interest for the same reason, since it penalises the threshold difference the leniency model is there to absorb.

One consequence of stratified estimation is worth stating because it is easy to get wrong. A stratum carrying large population weight but few adjudicated events contributes a high-variance ratio at high weight, so a partially filled panel gives an unstable estimate. The blind panel reported here is not in that regime: all 24 Ridgecrest strata carry at least six adjudicated events, and no stratum with fewer than five verdicts holds any weight. We know what a partially filled version of this design does, because Ridgecrest was first laid out as a 500-event single-reviewer pass whose interface is not used here (Supplementary Table 1): along that queue the weight held by strata with fewer than five verdicts was 81.9% after 140 adjudicated events, 7.2% after 300 and 1.5% after 375, so an interim estimate would have been unstable and would have understated the result. This is a property of the estimator, not of the reviewers: adjudication order does predict the raw verdict (+0.210 Spearman, p = 3e-05), but the association disappears once the stratum is controlled (likelihood-ratio $\chi^2 = 0.87$, p = 0.35), because the queue presented the hardest stratum first. Revision is a separate question, and on the blind panel it does not arise: 3 of 800 reviewer–event pairs were revisited and none changed class, so the reported numbers are the same whether the first or the last verdict is kept.

Note S8 | Scale selection and controls for the geometric statistics

Each of the three geometric statistics carries a scale with no default that travels between sequences, and each has controls that are reported but are not used to separate the score groups. Both are given here.

The correlation dimension: what is not controlled.

Network geometry is not removed from the score before D_2 is computed. The station count, the azimuthal gaps and the nearest-station distance are computed from the stations the associator actually assigned, so they record how clearly the event announced itself and not only how well the network could have seen it: a variance decomposition over spatial cells leaves 91 to 94% of the station-count variance inside cells, and within a fixed magnitude band and cell the station count tracks the measured signal-to-noise at rank correlation +0.49. Residualising on those columns removes evidence along with the confounder, and the residualised contrasts are reported in Fig. S4a as a deliberately over-strong floor. The control that addresses location quality without removing evidence is the reference control above.

Fault-segment fitting: choosing the two length scales.

Neither of E2F's two length scales carries a default that travels between sequences, so both are set per catalogue. The Hough discretisation defaults to 1/64 of the extent of the seismicity, which fragments a wide or diffuse plane, so 1/32 and 1/16 are scanned as well. The control scale is scanned over a grid anchored on the published optima, which run from 3.5 for a ~3 km fracture network to 100 for a ~500 km sequence. The pair is then chosen on the count of segments holding at least fifty events whose planarity lies in [0.8, 1], with event utilisation breaking ties. We do not use the released selection metric unmodified, because its scalar-moment criterion accepts every segment in all six of our catalogues and therefore only rewards fragmentation; the chosen scale and the full scan are reported for each catalogue (Table S10).

A second quantity, reported in Tables S10 and S11, is the fraction of a group's events lying in segments of at least fifty. A segment of six points in three dimensions is planar by construction, so segment planarity itself rewards fragmentation and is not used. The fifty-event floor is ours and not E2F's, although the contrasts are flat as it is varied from ten to two hundred (Table S11).

Groups within a catalogue are drawn to a common magnitude histogram in 0.2-unit bins, taken bin by bin as the smaller of the two thirds' counts, so that they are equal in size as well as in magnitude; matching one third to the other's histogram instead would leave the groups unequal, and a fraction computed over fewer events is not comparable. Five random draws to the same histogram give the null. Nothing else is controlled, for the reason set out under the correlation dimension. Location precision is not removed from the score either. The control applied is the reference control described below, which needs no error model. A position-error injection, which needs one and depends on a proxy for location error that is the disagreement between two location procedures and not the calibrated error of either, is retained in the Supplement with its question stated.

The double seismic zone: mode counting and the spatial controls.

Two further summaries are reported and neither is used to separate the groups. Kernel density estimation (Gaussian kernel, bandwidth factor 0.35, 400-point grid, local maxima whose prominence exceeds 12% of the global maximum) counts modes, but that count depends on the bandwidth: swept from 0.25 to 0.50 against three prominence thresholds, the two groups differ in 6 of 15 settings and agree in the rest. The Bayesian information criterion[28] of a two-component against a one-component mixture prefers two components in both groups by a similar margin. Both are reported because they are the conventional summaries and because their limitations are part of the result.

Two spatial controls are applied. The high-confirmability group is drawn to the low-confirmability group's own depth histogram in 5 km bins, and the comparison is repeated within one-degree latitude bands. Latitude is used instead of full three-dimensional position for a reason: at fixed latitude, longitude and depth the distance below the interface is almost determined, with cell identity accounting for 99% of its variance, so matching on all three would control the quantity being measured instead of a confounder of it.

Note S9 | The three-catalogue comparison: panels, covariates and pre-registration

From each of the two we drew a stratified panel of 200 events on the variables that catalogue records (magnitude and depth for both; for QTM also the relocation error and whether the event relocated with others), rendered them under the same blinding rules as the six original panels, on the vertical component with the channel code printed, and had one of the four original reviewers judge them through the same portal. A first pass on these two panels was rendered without the channel code, so a reviewer could not tell a horizontal component from a vertical one; those verdicts are quarantined in the archive and enter no analysis here. That reviewer's leniency term is already estimated from the crossed design, so the three arms can be compared on either of two label constructions: the four-reviewer consensus on our arm against the single reviewer on the new arms, or that reviewer's own blind verdicts on all three. We report both, and the like-for-like construction is the one quoted in the Results.

The comparison is restricted to the support the three panels share, i.e. the intersection of their time spans (4 July 17:40 to 16 July 22:12 UTC) and of their spatial extents (35.525 to 35.987°N, 117.750 to 117.254°W). Within that support the arms hold 93, 199 and 122 adjudicated events (ours, Shelly and QTM, respectively), with magnitude medians of 1.69, 1.19 and 1.31 and median times since the M7.1 of ~34, ~93 and ~62 h, so neither covariate can be assumed away. The confirmed fraction is therefore estimated from a logistic model of the verdict with terms for pipeline, magnitude and log time since the mainshock, and every arm is standardised to the pooled covariate distribution before contrasts are taken, so that no contrast is read off a range one catalogue does not occupy. Contrasts are reported as adjusted risk differences with 95% intervals from 600 bootstrap resamples drawn within arm. In addition, the panel's unresolved verdicts are handled under all three conventions (excluded, counted rejected, counted confirmed) and the bracket is the result.

The decision rule was fixed and committed before either new panel was reviewed. The substantive margin is 13 percentage points, set to the design's own minimum detectable difference at 80% power and not to a round number; a 10-point margin was considered and rejected because power at that margin is 58 to 75% across the three pairs. Precision is called a pipeline property if any pairwise adjusted difference reaches 13 points with a 95% interval excluding zero, and sequence-dominated if all three pairwise 90% intervals lie inside ± 13 points. The pre-registration also required that the arms be brought onto a common covariate support without trimming more than a quarter of any arm. Trimming to the joint 5th to 95th magnitude percentiles (0.43 to 2.45) removes 17% of Shelly, 16% of QTM and 35% of our arm, because our panel was stratified to carry more events above M2.45 than the other two hold. That gate is therefore tripped on one arm. We report it as a protocol deviation rather than as a caveat: the pre-registered rule makes the trimmed comparison the confirmatory one, and because the trim removes more than the quarter the rule allows, the three-catalogue contrast is reported here as exploratory. Both the trimmed and the untrimmed results are given, and they agree in every cell. Verdicts recorded through a non-blind interface by one reviewer on this panel are excluded from every analysis in this paper; the count of 93 uses blind verdicts only.

Note S10 | The off-fault tail: confounders, and how the reference control was read

Two confounders are removed before the tail is read. Reference-matched events are systematically larger than the catalogue as a whole (median M1.45 against M0.69), so every comparison involving them is made inside the reference subset's own 5th to 95th magnitude window, and the full-catalogue contrast is recomputed inside that window instead of being carried over. And whether an event reached the regional catalogue depends on when it happened, because analyst completeness degrades in the coda for the same reason the score does: the match rate inside the fixed magnitude window is 58% before the M7.1, ~40% through the first day and 21 to 28% thereafter. The cutoff of 24 h was chosen from that inclusion curve alone, before any fault-distance result was computed, and the comparison is made beyond it.

The reference control itself removes confirmability as an explanation by construction. Restricting to the detections that the human-reviewed regional catalogue independently contains, none of which can be false, and repeating the score split inside that subset asks whether the contrast can be produced without any false detection at all. The reading was fixed before the result: a contrast among independently catalogued events comparable to the full catalogue's means location and observational quality alone can produce it; a contrast near zero while the full catalogue's stays large means they cannot; a subset too sparse to estimate the statistic over the same scaling range means the control is uninformative. A 5 km match radius is itself location-dependent, since a real event located badly enough fails to match and is then counted as non-reference, which would manufacture the contrast being tested; the control is therefore repeated with the radius widened to 15 km and the time window tightened to 1 s, and the tail does not reappear (Fig. S5c).

The two geometric statistics answer this control differently, and that difference is reported and not reconciled. For the correlation dimension, 75% of the Ridgecrest contrast is reproduced among independently catalogued events (+0.37 against +0.50), and 64% at the tightest match (1 s, 2 km); D_2 is accordingly presented as evidence that catalogue quality structures a geometric statistic and not as evidence of contamination, and a position-error injection is retained in the Supplement with its question stated, since it asks whether one modelled error process can reproduce the contrast and not whether false detections are necessary for it. For the fault distance, 17% of the contrast is reproduced (+0.07 km against +0.41 km), the fraction beyond 10 km falls from 6.7% to 0.4%, and the result is unchanged beyond 24 h. The tail is therefore concentrated in detections the human-reviewed catalogue does not contain. Testing whether those are false requires the panel's own verdicts, and a fitted-fault distance regressed on the consensus verdict with magnitude and log time as covariates gives $\log_{10}$ differences of +0.05 (false against real, n = 27), +0.02 (uncertain, n = 49) and +0.03 (pooled, n = 76), all positive and none resolved; against a full-catalogue effect of about 0.15 in $\log_{10}$ and a standard error of 0.11, that is a statement about power and not about absence. The tail is therefore attributed to machine-only detections.

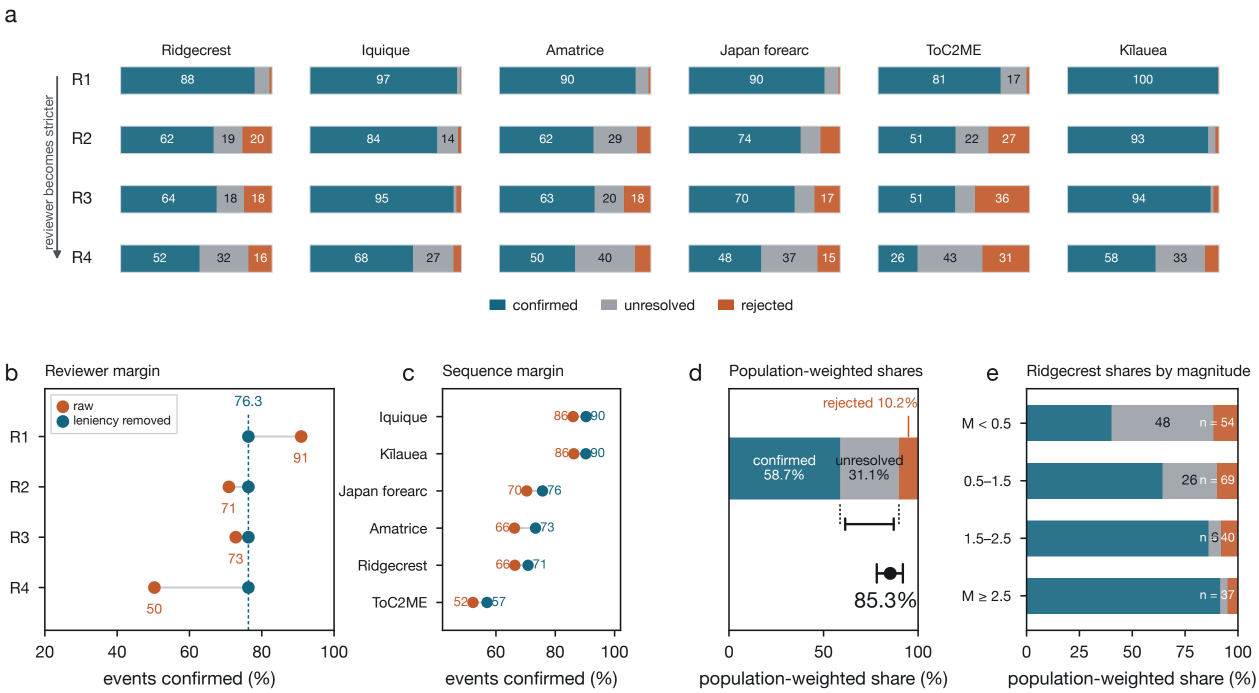

Fig. S1 | The raw verdicts and the reviewer effect. **a**, The 4,800 verdicts as a grid: one row per reviewer, one column per catalogue, each cell a stacked bar of confirmed (blue), unresolved (grey) and rejected (orange) verdicts on that catalogue's 200 events. Reviewers are labelled R1 to R4 in order of leniency (Table S5 maps the labels to the authors). Two effects are visible before any model is applied: every reviewer finds ToC2ME hardest and Kīlauea and Iquique easiest, and the reviewers hold their order at the ends, R1 the most lenient and R4 the strictest on every catalogue, with R2 and R3 changing places between them. **b**, Raw confirmation rates per reviewer (orange) and the same rates after removing each reviewer's fitted leniency term (blue). The leniency model treats a verdict as a comparison between the event's latent quality and a threshold that differs by reviewer; it is the reviewer analogue of a station correction in earthquake location, one number per observer that absorbs a systematic offset. Because every reviewer judged every event, the four corrected rates coincide by construction; what the fit establishes is that four such terms reproduce 89.5% of the individual verdicts. **c**, Raw and corrected confirmation rates per catalogue. Removing leniency raises every catalogue by 4 to 7 points and leaves the ordering essentially intact; the only two pairs that change places, Kīlauea with Iquique and Ridgecrest with Amatrice, are separated by less than a point in the raw rates. **d**, The design-weighted composition of the Ridgecrest catalogue implied by the consensus labels: 58.7% confirmed, 31.1% unresolved and 10.2% rejected. The bracket is what the confirmed share becomes when the unresolved share is assigned first to rejected and then to confirmed, and the dot is the confirmed fraction among decided events, 85.3%. **e**, The same design-weighted shares by magnitude bin at Ridgecrest: the undecided share is 3% above M2.5 and 48% below M0.5, so the range in Fig. 2b is set by the smallest events, which are the ones a machine catalogue adds.

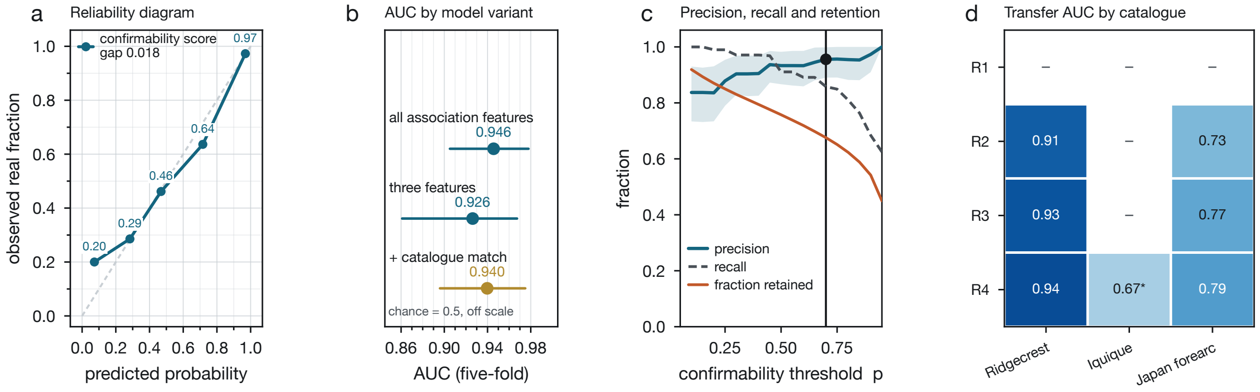

Fig. S2 | The score that reproduces the panel. **a**, Reliability diagram for the confirmation probability at Ridgecrest: for events binned by their predicted probability, the fraction the panel confirmed against the mean prediction, with the one-to-one line. The model is an ℓ2-regularised logistic regression on the panel's confirmed-against-rejected label with unresolved events excluded, fitted to seven association-stage features (phase count, station count, move-out residual, primary and secondary azimuthal gap, nearest-station distance and magnitude) under five-fold cross-validation, so every prediction shown was made for an event the model did not see. Because unresolved events are excluded, the quantity estimated is the chance the panel would confirm an event among events it was willing to decide, not the chance the event is real. The expected calibration error, design-weighted over five equal-width bins, is 0.040, against 0.145 to 0.499 for the substitutes in common use (Note S1). **b**, The ranking: how often a panel-confirmed event scores above a panel-rejected one (the area under the receiver operating curve, AUC), 0.946 for the full model, 0.926 for three features only, and 0.940 with the reference-catalogue match added. **c**, Retention tiers: keeping events whose confirmation probability is at or above a threshold, the fraction of the catalogue retained, and the precision and recall of what is kept against the panel's verdicts; at 0.7 the tier retains 67.6% of the catalogue at a precision of 96% and a recall of 86%. **d**, Transfer: the area under the curve of the Ridgecrest-fitted score against each reviewer's own blind verdicts, one cell per reviewer and catalogue. A dash marks a unit in which that reviewer returned fewer than ten rejections, too few for the statistic to mean anything, and an asterisk marks an interval that reaches chance. Reviewers are labelled as in Fig. S1.

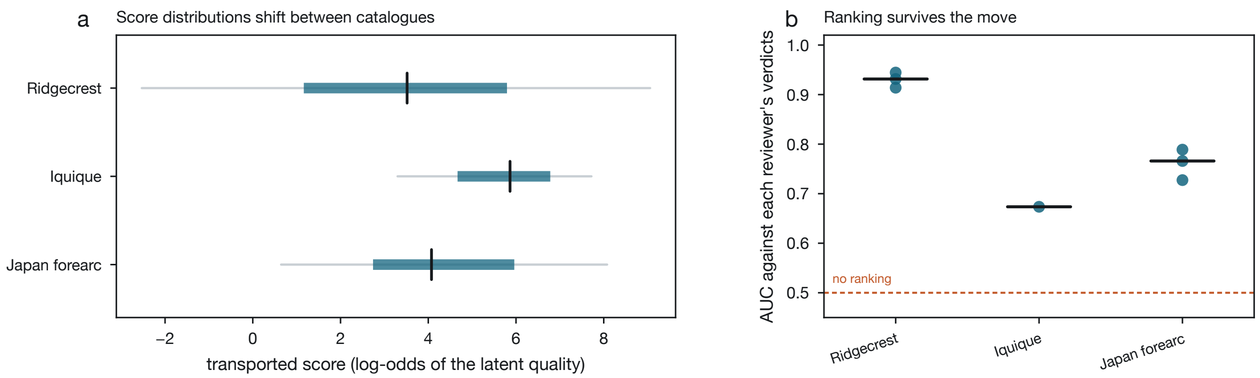

Fig. S3 | Transfer of the ranking between sequences. **a**, The distribution of the Ridgecrest-fitted score when it is applied unchanged to each catalogue: box, the interquartile range; line, the median; whiskers, the 2nd to 98th percentiles. The distributions sit at different levels, which is why the score transfers as a ranking and a threshold chosen in one sequence does not carry to another. **b**, The ranking itself. Each point is the AUC of that score against one reviewer's own blind verdicts on one catalogue, and the bar is the median over the reviewers of that catalogue; a reviewer who returned fewer than ten false verdicts is omitted, because the negative class is then too small for the statistic to mean anything (Table S4). Within Ridgecrest, where the score was fitted, the median AUC is 0.93; in the two sequences the model never saw it is 0.75, above chance for all three retained reviewers in Japan and not resolved at Iquique, where one reviewer survives the cut.

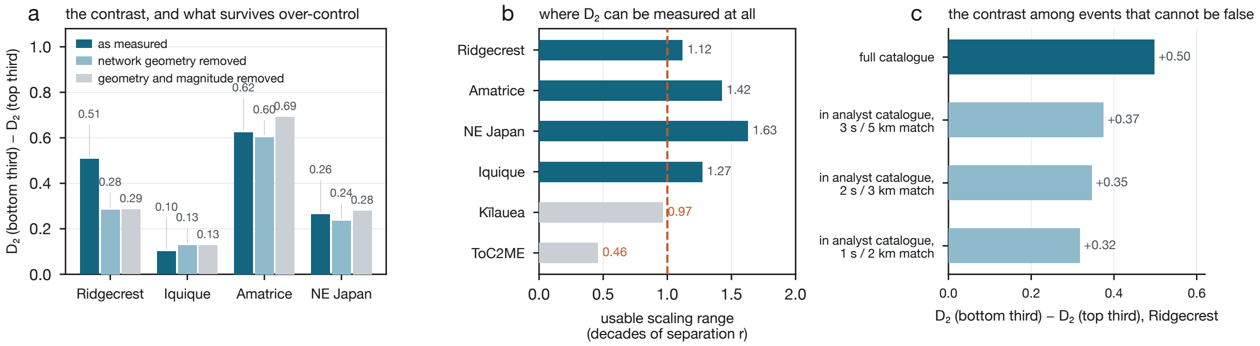

Fig. S4 | The correlation dimension in every catalogue where it exists. **a**, The difference in D_2 between the bottom and top quartiles by score for the four catalogues with a usable scaling range, as measured (dark) and after two deliberately over-strong controls that residualise the score on the network-geometry features and on magnitude (light). The controls remove evidence along with the confounder, since the station count in these catalogues tracks the measured signal-to-noise and not the position of the event (Methods), and are shown as a floor and not as the estimate. **b**, The usable scaling range in decades of separation for all six sequence catalogues; a range under one decade, the dashed line, is declined before the result is seen, which excludes Kīlauea (0.97 decades) and ToC2ME (0.46). **c**, The reference control: the D_2 contrast in the full Ridgecrest catalogue, +0.50, against the contrast among only the 20,588 detections the human regional catalogue independently contains, +0.37, with the two tighter match tolerances beside it. Three quarters of the contrast survives among events that cannot be false, so D_2 is reported as evidence that catalogue quality structures a geometric statistic and not as evidence of contamination.

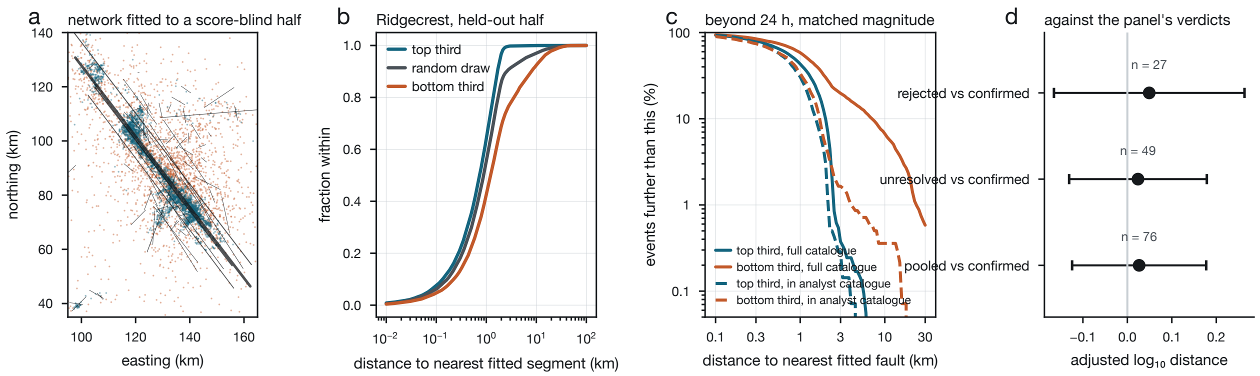

Fig. S5 | The fault-distance statistic and its controls. **a**, The Ridgecrest fault network fitted to the score-blind half, in map view, with the top and bottom thirds of the held-out half. Segments are drawn as their major axis; the method resolves strikes but not dips on these data, and the comparison requires only that the network was placed without reference to the score. **b**, The cumulative distribution of distance to the nearest fitted segment for the top third, the bottom third and a random draw of the same size; the random draw sits between the two thirds in every one of the six catalogues. The two thirds part at about 2 km: beyond 3 km lie 20% of the bottom third and 0.4% of the top, beyond 5 km 13.7% against 0.15% (a ratio of ~91, 95% CI 53 to 244), and beyond 8 km 9% against none of the 5,326 events in the top third, so about a fifth of the bottom third sits off every fitted fault. **c**, The reference control for the off-fault tail: the fraction of each third beyond a given distance in the full catalogue (solid) and among independently catalogued events only (dashed), beyond 24 h and at matched magnitude. The tail all but vanishes among independently catalogued events, and it does not reappear when the match radius is widened to 15 km to admit badly located real events. **d**, Fitted-fault distance against the panel's own verdicts at Ridgecrest, adjusted for magnitude and time since the mainshock; false, uncertain and pooled non-confirmed events all sit further from faults than confirmed ones, but none of the three contrasts is resolved at 200 events, and the tail is therefore attributed to machine-only detections and not to false ones.

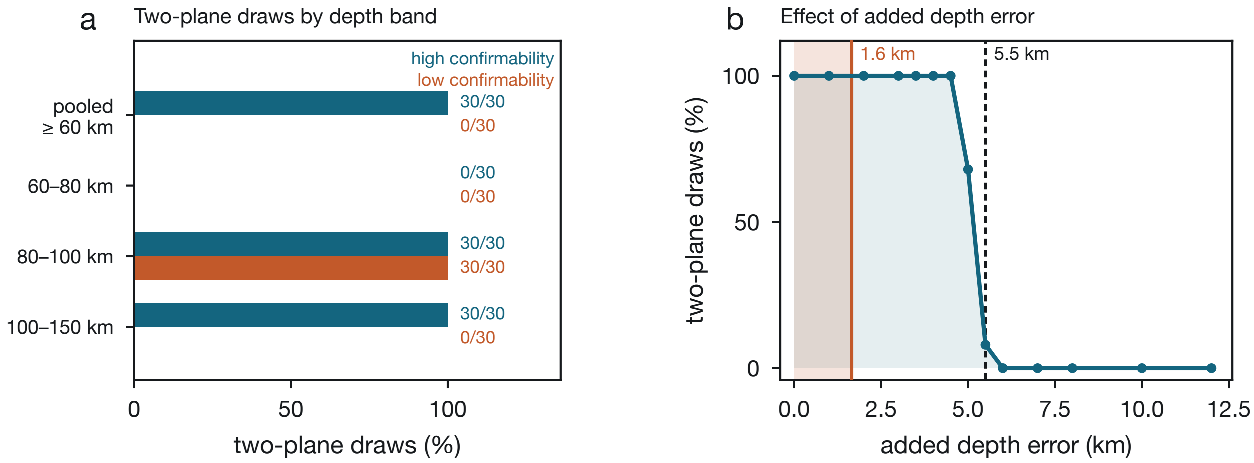

Fig. S6 | Controls for the double seismic zone. **a**, The fraction of resampled draws in which a kernel-density estimate of the distance below the interface has two or more modes, by depth band, for the top and bottom score quartiles. Mode counting, not the mixture criterion of Fig. 4b, is the statistic here. Both quartiles resolve two planes at 80 to 100 km and neither does at 60 to 80 km, where the planes are only 8.5 km apart. **b**, Depth-error injection: Gaussian noise of increasing standard deviation added to the depths of the top quartile, and the fraction of draws that still resolve two planes. Resolution is intact to 4.5 km, falls below half the draws at 5.5 km and is gone by 6 km; the bottom quartile's own excess depth uncertainty, from the catalogue's reported errors, is 1.65 km (orange line). This bounds the blur explanation under the reported uncertainties and does not exclude it.

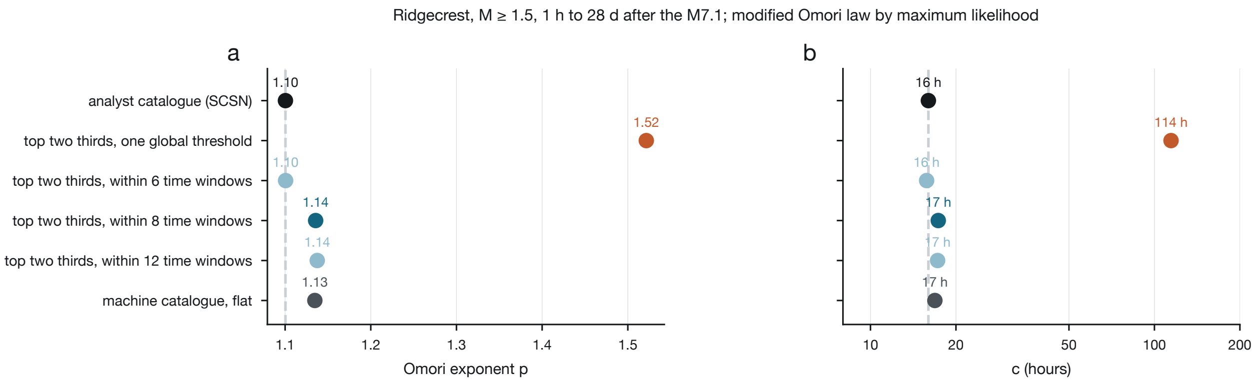

Fig. S7 | What a global tier does to the aftershock decay. The modified Omori law, $n(t) \propto (t+c)^{-p}$, fitted by maximum likelihood to Ridgecrest aftershocks above M1.5 from 1 h to 28 days after the M7.1, for the human-reviewed regional catalogue, for the flat machine catalogue, for the machine catalogue keeping the top two thirds by one global score threshold, and for the machine catalogue keeping the top two thirds within each of six, eight or twelve log-spaced time windows. The exponent p sets how fast aftershocks decay and c is the time before the decay begins, which absorbs early incompleteness. The score is systematically lower in the hours after a mainshock because the coda is busy, so a global threshold removes early aftershocks preferentially: the fit then has to explain a missing early population, and does so by pushing c from about 16 h to about 114 h and p from 1.10 to 1.52. A threshold set within time windows leaves both where the human-reviewed catalogue puts them.

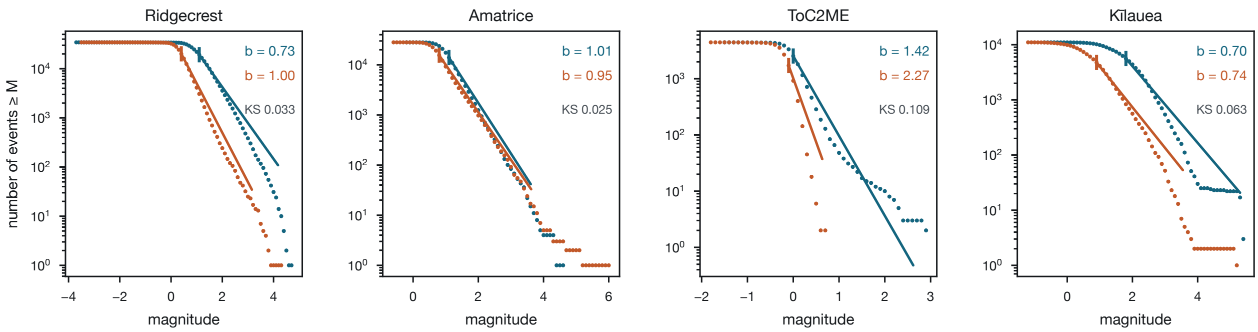

Fig. S8 | Frequency–magnitude distributions by score. Cumulative frequency–magnitude distributions for the top (blue) and bottom (orange) score quartiles of the four catalogues whose magnitudes span enough range to fit one, with the Gutenberg–Richter b-value fitted above each group's own completeness magnitude (tick) and the Kolmogorov–Smirnov distance of the low-ranked group from its own fitted line. At Ridgecrest and Amatrice the low-ranked population is itself close to a straight line (b = 1.00 and 0.95, KS 0.033 and 0.025), so a frequency–magnitude diagnostic would not have identified it; that is why the audit returns to the waveforms. At ToC2ME the low-ranked group departs further (b = 2.27), which is consistent with its being the catalogue the panel confirms least.